PREPARATION AND VISUALIZATION OF INDIVIDUAL ACTIN FILAMENTS
USING ATOMIC FORCE MICROSCOPY FOR THE STUDY OF ACTIN/DNA
HYDROGEL COMPLEXES

by

Joshua D Kennedy

A thesis submitted to the faculty of
The University of North Carolina at Charlotte
in partial fulfillment of the requirements
for the degree of Master of Science in
Applied Physics

Charlotte

2019

Approved by:

_____
Dr. Yuri Nesmelov

_____
Dr. Yasin Raja

_____
Dr. Nathaniel Fried

ABSTRACT

JOSHUA D. KENNEDY. Preparation and visualization of individual actin filaments using atomic force microscopy for the study of actin/DNA hydrogel complexes. (under the direction of DR. YURI NESMELOV)

A protocol of sample preparation for the visualization of single actin filaments at the nanoscale using atomic force microscopy for use in studies of engineered actin/DNA conjugated hydrogel complexes was developed. Hydrogels are cross-linked networks of hydrophilic monomers synthesized into polymers which behave as solids at the macroscale but exhibit fluid-like properties at the microscale, containing interstitial spaces which swell with water, allowing water content to multiply to thousands of times their weight, resulting in viscoelastic mechanical properties. F-actin and DNA have both exhibited potential for use in biocompatible engineered hydrogel applications. A procedure for actin sample preparation was developed which utilized aminopropyltriethoxysilane (APTES) to covalently attach a charged amine group (*N*, *N*-diisopropylethylamine) to mica substrates through vapor deposition in a desiccator that had been purged with nitrogen before deposition of F-actin samples and imaging. This method reliably produced images of individual actin filaments suitable for studies of engineered DNA/actin hydrogels. In addition, initial work was begun on the formation of two different potential DNA/actin conjugate complexes using complementary DNA oligomers combined with crosslinking molecules (SMPB) and actin. Initial results

showed differences in average filament diameters and average persistence lengths in

conjugate samples compared to actin samples.

ACKNOWLEDGEMENTS

TABLE OF CONTENTS

LIST OF TABLES

LIST OF FIGURES

CHAPTER 1. INTRODUCTION

Our laboratory is interested in developing a protocol of sample preparation for the visualization of single actin filaments at the nanoscale for future studies of engineered actin/DNA hydrogels. In the early 1950s Otto Wichterle and Drahoslav Lím from the

Figure 1: Otto Wicterle (left) and Drahoslav Lim (right), creators of soft permeable contact lenses and hydrogel innovators.

Prague Institute of Chemical Technology (who would both soon move to the Institute of Macromolecular Chemistry at the Czechoslovak Academy of Sciences in Prague, and are pictured in figure 1) initiated a research program to design polymers for medical use which would fulfill criteria for biocompatibility (Kopecek, 2009). These experiments would eventually lead to the development of soft contact lenses, and this work would mark the beginning of synthesized biocompatible hydrogel research. Hydrogels or polymer gels are cross-linked networks of hydrophilic monomers synthesized into polymers which behave as solids at the macroscale but exhibit fluid-like properties such as molecular diffusion at the microscale. These molecular networks of polymer gels contain interstitial spaces which swell with water allowing a high water content, sometimes hundreds to thousands of times their weight, and results in viscoelastic mechanical properties that vary depending on the components of the engineered gel (Kawamura, 2016).

Research is currently being conducted on many potential hydrogel applications including biocompatible tissue replacement, permanent cartilage implants, and engineered extracellular matrix for artificial organs. Controlled growth modes are being studied which can create complex three dimensional hydrogel architectures through successful biomimetics of tissue morphogenesis in animals and plants. Architectures which were developed in one study include a leaf with assembled capillaries (pictured in figure 2) as well as the human airway; this was accomplished by controlling oxygen diffusion-regulated polymerization and introducing mechanical constraints in the form of a small wire. (Changjin Huang, 2018). The ability of hydrophilic polymers to be used as thin films, scaffolds, or nanoparticles has convinced some researchers that hydrogel systems have additional potential use in biosensors, DNA microarrays, and biomedical imaging (Langer, 2006). Alternatively, some hydrogel products such as

Figure 2 A hydrogel leaf developed in a cooperative effort between Nanyang Technological University, Singapore (NTU Singapore) and Carnegie Mellon University (CMU)

super-absorbent diapers, hygiene products, soft contact lenses, tissue engineering scaffolding, drug delivery systems, and wound dressings are already being manufactured and are widely available in the marketplace (Enrica Caló, 2014). Despite this, many more hydrogel products have been designed and even patented than have been commercialized,

especially in regards to drug delivery and tissue engineering. High production costs are a chief reason for the delay of further commercialization in these sectors.

Since both natural and synthetic polymers can be physically or chemically crosslinked to form hydrogels, there exist two types of hydrogels, synthetic hydrogels and biological hydrogels. Since we are interested in the development of Actin/DNA hydrogels, this work will focus on biological hydrogels. Most of a living organism consists of soft tissue biological hydrogels such as the extracellular matrix which regulate the transportation of water, ions, and other substances, sustaining vital functions with controlled viscoelastic properties. Although these hydrogel-based filters which use selective diffusion are integral parts of biology, clear concepts of how their barrier function is controlled on a microscopic level are still missing (Oliver Lieleg, 2011). This biological functionality of selective exchange observed at the macroscale in the extracellular
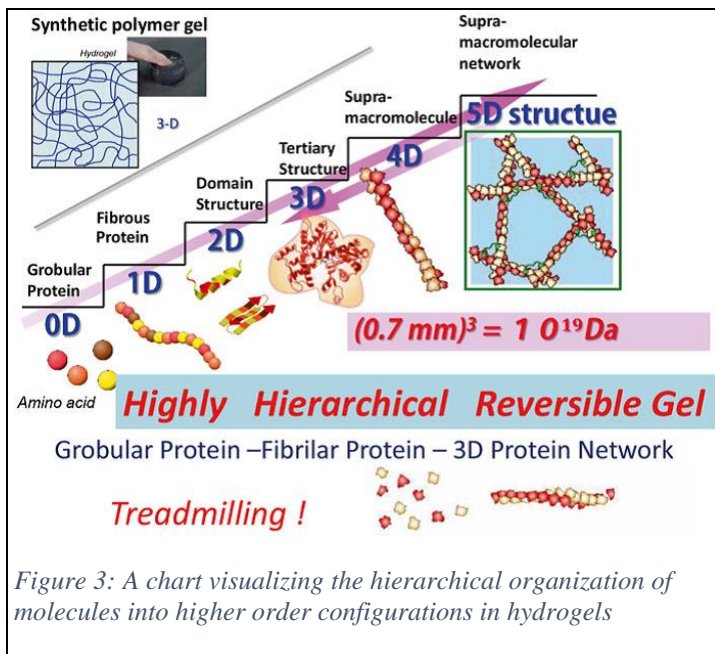
Figure 3: A chart visualizing the hierarchical organization of molecules into higher order configurations in hydrogels

matrix (as well as in mucus and in the biopolymer layer of the nuclear pore), is an emergent property of the hierarchical organization of molecular networks into higher ordered configurations. The search for these kinds of high order functional emergent properties is

one of the critical targets of polymer gel study. This hierarchical ordering of molecular

structures in hydrogels can be visualized in figure 3.

The muscle protein actin is one biomolecule which has shown potential for gel

development with emergent function. Actin is the most abundant protein in eukaryotic

cells, and is found in monomer form (globular actin or g-actin) and polymer form

(filamentous actin or f-actin). Filamentous actin is a polymer composed of g-actin
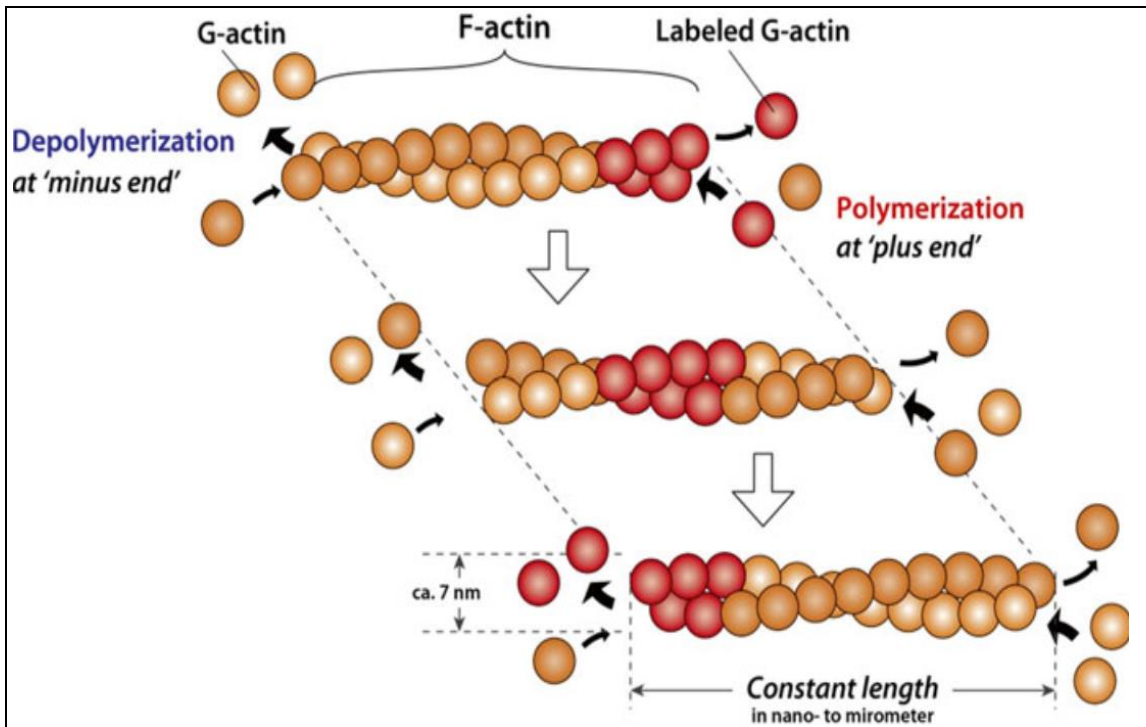
Figure 4: Diagram of F-actin "treadmilling," wherein total polymer length remains fixed but the G-actin monomers move around like an athletic treadmill. Treadmilling has been shown to lead to higher order emergent function in actin polymer gels.

monomers which can be microns long but has a diameter of a few nanometers and is

responsible for muscular contraction in conjunction with myosin. F-actin has a polar

structure which leads to differences in polymerization rates at both of the ends of the actin

filaments and can create a state in which g-actin monomers depolymerize at one end and

polymerize at the other, resulting in a motile effect known as "treadmilling," where

polymer length remains fixed but the actin monomers move around like an athletic treadmill (shown in figure 4). This treadmilling effect of actin has been shown to be responsible for several emergent functions in lab produced actin gels including reversible solid to gel transitions, self-healing functionality, oscillatory properties, and high mechanical strength (Kawamura, 2016). Furthermore, muscle contraction in various organisms is an evident emergent function of actin in conjunction with myosin and related muscle proteins such as troponin and tropomyosin. Therefore, actin appears to be a good candidate when searching for a biomolecule which could provide emergent functionality in an engineered polymer gel.

DNA is another biomolecule which has similarly shown potential for emergent function in engineered hydrogels. DNA is found in all prokaryotic and eukaryotic cells as well as many viruses and is the double helix stranded polymer which codes genetic information for the transmission of acquired traits (Brittanica, 2018). The fact that DNA is so prolific in living organisms makes it an attractive option for applications requiring biocompatibility. DNA is also useful in the sense that it can be manipulated by many different molecular tools including enzymes, and displays interesting emergent functionality such as damage response/lesion healing (Stephen P. Jackson, 2009). In fact, three-dimensional crosslinked DNA hydrogels have already been constructed which are biocompatible, biodegradable, inexpensive to fabricate, and easily molded into desired shapes and sizes (Soong Ho Um, 2006). DNA hydrogels which take advantage of enzymatic interactions as well as thermal responses to induce reversible solid to gel transformations have also already been created in the laboratory (Liu, 2010). Another

5

aspect of DNA which makes it desirable for engineering polymer gels is the complimentary nature of individual DNA sequences. For example our lab is interested in whether the activity of combining complementary DNA strands which have been crosslinked to filamentous actin could result in reversible solid to gel transformations by enzymatic interactions such as introduction to helicase, which would cause the complementary DNA oligonucleotides to "zip" while in the presence of each other or "unzip" in the presence of the enzyme.

F-actin and DNA have both been shown to exhibit emergent functionality and potential for use in robust biocompatible engineered hydrogel applications. Additionally, the double helix structure of DNA is similar to the helical structure of filamentous actin strands as they form into bundles of macromolecular filaments. It is reasonable to suspect that the similar structure of the molecules could lead to interesting physical conformations at higher ordered configurations leading to the discovery of emergent functionalities. For these reasons, this work will be concentrated on developing a protocol of sample preparation for the visualization of single actin filaments at the nanoscale for the study of novel engineered actin/DNA hydrogels, as well as preliminary attempts at engineering actin/DNA crosslinked hydrogel molecules.

CHAPTER 2. MATERIALS AND METHODS

2.1 Imaging Modalities

Before attempting to synthesize novel DNA/actin hydrogels, a protocol for nanoscale imaging of singular actin filaments is first required to calibrate and parameterize the experimental setup to later confirm, resolve, and analyze the formation of the DNA/actin polymer gel molecules. If functionally resolved images of single actin filaments can reliably be reproduced then this level of resolution should be adequate for the visualization of the engineered gel molecules, as we should be able to detect structural changes associated with the filaments interacting with both the crosslinkers and DNA oligomers. Single actin filaments can be a few micrometers long but have a relatively small diameter of just a few nanometers. These dimensions make imaging single filaments rather difficult, and make the choice of imaging modality paramount in our endeavor.
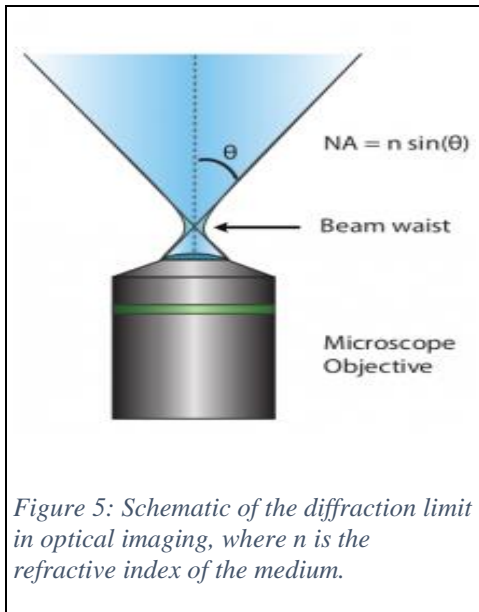
Figure 5: Schematic of the diffraction limit in optical imaging, where n is the refractive index of the medium.

Traditional optical imaging systems have been a tremendously valuable research tool, but they possess an inherent resolution limit that is based upon the diffraction of light. This is known as the diffraction limit of Abbe's diffraction limit after its discoverer Ernst Karl Abbe, a German physicist and optical scientist. The resolution limit is proportional to the wavelength of the illuminating light and inversely proportional to double the

numerical aperture. This formulation is shown in equation 1 and an illustrated schematic of the diffraction limit (d) can be seen in figure 5, where λ is the wavelength of light used, NA is the numerical aperture of the objective, n is the index of refraction of the medium surrounding the lens, and theta is the maximum half-angle of the cone of light entering or leaving the lens.

$$\text{Equation 1:} \qquad d = \frac{\lambda}{2\text{NA}} = \frac{\lambda}{2n\sin\theta}$$

If we assume a visible green light for illumination (~ 530 nm wavelength) and a maximum numerical aperture of 2 (which is much higher than likely), then the result is a resolution limit of about 133 nm. Therefore the diffraction limit for optical imaging systems does not allow for the imaging of singular actin filaments, which have a diameter of just a few nanometers. Attempts at imaging larger F-actin bundles with fluorescence microscopy have been completed with relative success (A. Ott, 1993) (Blancaflor, 2004). An example of fluorescence microscopy imaging of labelled F-actin is shown in Figure 6. We can see bundles of strand-like formations which are networked together and have filamentous
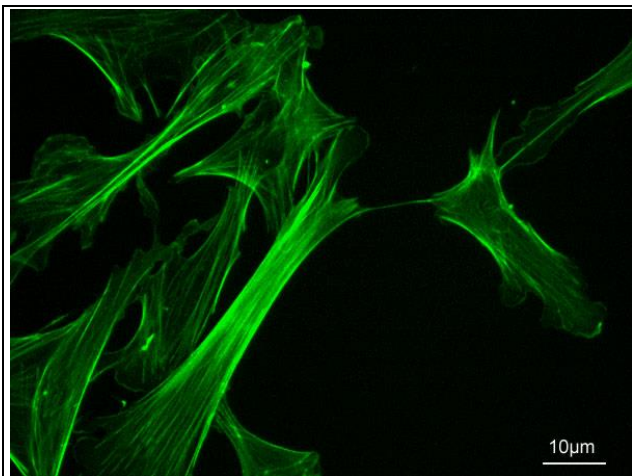
Figure 6: Fluorescence microscopy image of labelled F-actin in rat fibroblasts.

characteristics, however if we are trying to observe singular filaments forming objects on the scale of a few nanometers, then fluorescence microscopy and optical systems in general

8

are insufficient. Similarly advances in EM, X-ray diffraction, fluorescence, and single molecule techniques have provided a wealth of information about the modulation of the F-actin structure and its regulation by actin binding proteins (ABPs), but the technological limitations of these approaches in retrieving molecular level information about structural changes due to interactions at the nanoscale make them poor candidates for our studies (Shivani Sharma, 2013). However, there exists imaging modalities which can resolve beyond the optical diffraction limit into the nanoscale, and indeed some that have already been used to image F-actin. Atomic force microscopy (AFM) for instance is a nanoscale imaging modality which has been used to resolve actin filaments in several studies (Marina Naldi, 2009) (Akihiro Narita, 2016) (Shivani Sharma, 2013) (Monika Fritz, 1995), and one that was readily available in-house for this work. It is this reasoning which led to the decision to attempt to utilize atomic force microscopy to resolve single actin filaments at the nanoscale for our experimental protocol.

2.2 Atomic Force Microscopy Theory

This section will be an introduction to the theory behind atomic force microscopy and how it works. Atomic force microscopy is a type of scanning probe microscopy (SPM) which is capable of high resolution nanoscale imaging. Scanning probe microscopes are instruments which create images using a
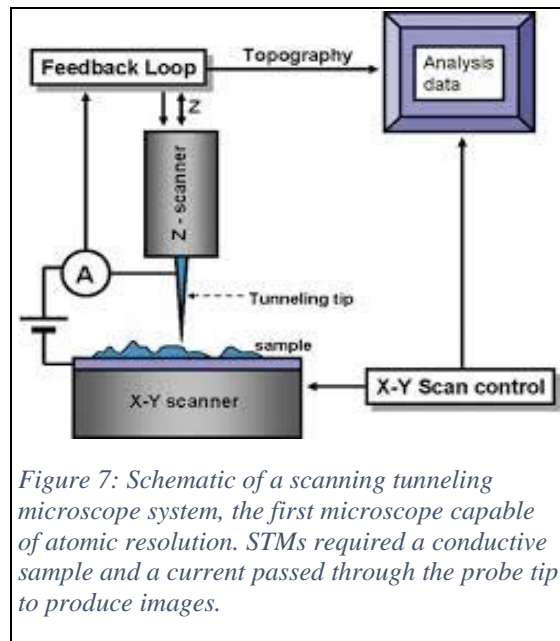
Figure 7: Schematic of a scanning tunneling microscope system, the first microscope capable of atomic resolution. STMs required a conductive sample and a current passed through the probe tip to produce images.

physical probe to feel the surface of a sample and collect positional data related to the probe (Wiesendanger, 1994). Most SPMs rely on a sharp tip attached to a computer-controlled z-scanner to probe the morphology of the surface. One of the first SPMs developed was the scanning tunneling microscope (also the first microscope capable of atomic resolution, a schematic of which can be seen in figure 7), which relies on the conductivity of the sample and a current being passed through the tip in order to gather information about the surface by means of interactions with the probe (Bruker, 2019). Like most SPMs, the AFM also uses a very sharp tip with a radius of curvature between 5 and 10 nanometers long attached to an adjustable z-controller to probe and map the morphology of a sample surface, but unlike the scanning tunneling microscope and other SPMs, atomic force microscopy does not rely on the sample to be conductive nor is it necessary to measure a current between the surface and the tip to produce an image.

Atomic force microscopes create images using a physical microscale cantilever set at a low spring constant between 20-100 N/m to probe the surface of a sample on a piezoelectric scanner and collect positional data about the tip which normally constitutes an array of points that can be reconstructed into a surface image and analyzed. The spring constant and displacement of the cantilever are described by Hooke's law (Hooke, 1678), represented in equation 2, wherein the force needed to compress or extend a spring scales linearly with displacement (x) and spring stiffness (k) (M Kopycinska-Müller, 2006).

$$\text{Equation 2:} \qquad F = -kx$$

The positional data about the tip is collected by reflecting a red laser beam off of the back of a mirror on the cantilever tip and onto the surface of a position-sensitive sectional photodiode detector. A basic schematic of this setup is presented in figure 8. Forces acting between the sharp probe tip and sample placed in close contact result in a measurable deformation of the cantilever to
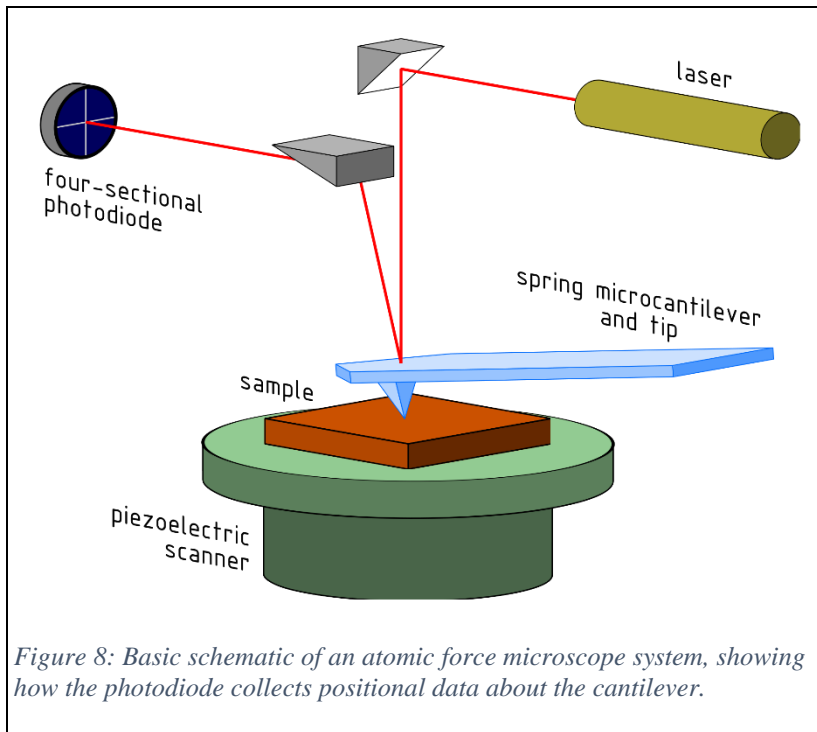
Figure 8: Basic schematic of an atomic force microscope system, showing how the photodiode collects positional data about the cantilever.

which the probe is attached (F. L. Leite, 2007). As the cantilever is displaced, the reflected light beam will also be displaced on the surface of the sectional photodiode. In this way, the attractive and repulsive interatomic forces between the tip and sample may be measured by a computer system to produce images. In the case of sample- tip interaction in AFM, the attractive forces would be due to the inherent molecular Van der Waals forces present between the sample and the tip. Van der Waals forces are weak attractive forces that arise from the interaction of electric dipole moments in uncharged molecules (I.E.Dzyaloshinskii, 1992). The repulsive forces acting between the sample and the tip are due to columbic interactions that occur between any two atoms or molecules when they

11

approach so closely that their electron orbitals begin to overlap; this is the result of the Pauli Exclusion Principle (F. L. Leite, 2007).

2.3 Modes of Operation

There are several modes of operation possible in atomic force microscopy, including contact mode, non-contact mode, and tapping mode (a graphic representation is shown in figure 9). In contact mode the deflection of the cantilever is sensed and compared in a DC feedback amplifier to some desired value of deflection. If the measured deflection is different from the desired value the feedback amplifier applies a voltage to the piezo stage to raise or lower the sample relative to the cantilever to restore the desired value of deflection, so that the voltage that the feedback amplifier applies to the stage can be a measurement of the height of features on the sample surface (Li, 1997). When operating in contact mode the cantilever tip remains in contact with the sample surface during the scan. Contact mode has a faster scan speed relative to the other modes, reduces Van der Waals forces, and can measure lateral forces due to the dragging effect. Alternatively, the constant lateral frictional forces incident on

Figure 9: Graphic representation of the modes of operation in AFM. (a) contact mode (b) non-contact mode (c) tapping mode

12
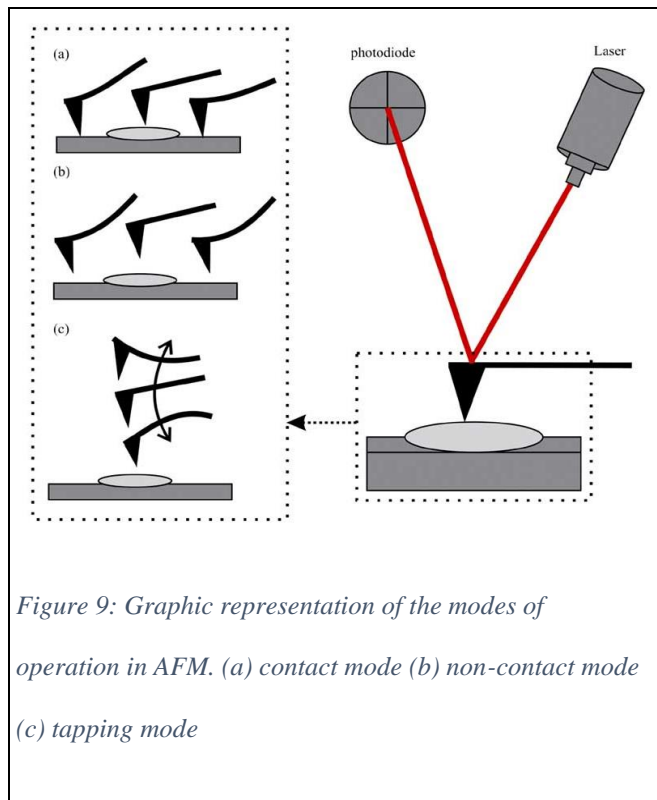
the surface can cause scraping and damage to the sample, dull the cantilever tip, and sometimes distort data by causing artifacts in the produced image. Furthermore, under ambient conditions water vapor and gasses from the air can deposit on the sample surface forming a thin film liquid meniscus layer (Hansma, 1990). The surface tension of this meniscus layer can then pull the probe tip towards its surface, distorting force measurements.

Non-contact mode keeps the cantilever tip oscillating at its resonant frequency as the cantilever tip approaches (but never comes into contact with) the sample surface. The distance between the tip and sample in non-contact mode is about 2-3 nm. As the cantilever draws near to the surface its natural frequency will experience a slight measurable shift (Y. Martin, 1987). As figure 10 illustrates, attractive forces will shift the resonant
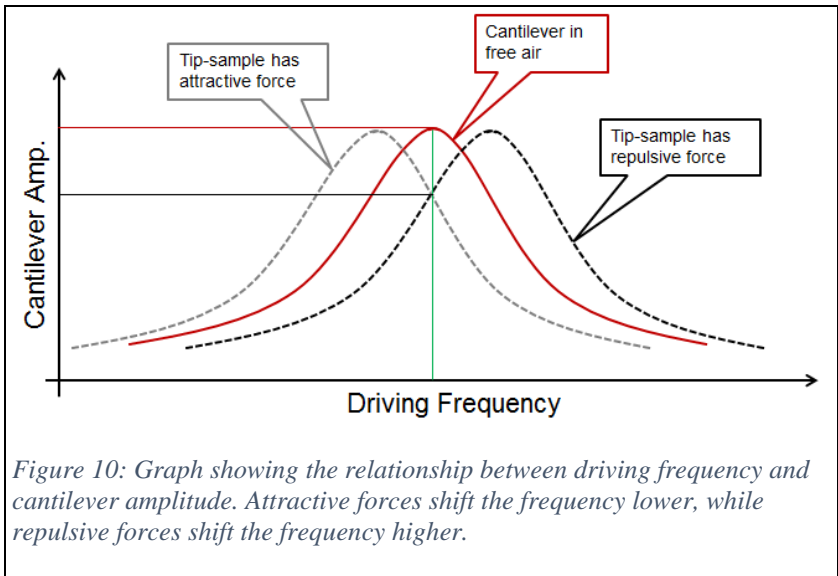
Figure 10: Graph showing the relationship between driving frequency and cantilever amplitude. Attractive forces shift the frequency lower, while repulsive forces shift the frequency higher.

frequency of the cantilever lower, and repulsive forces will shift the cantilever resonant frequency higher (Bruker, TappingMode AFM, 2010). These frequency changes are monitored by a z-controller system feedback loop and used to control the distance between the tip and the sample. In non-contact mode the tip-sample distance must be maintained at

a constant value to avoid crashing the tip into the surface. If the probe accidentally crashes into the sample, the tip can stick to the surface due to the force of the liquid meniscus layer and prevent oscillation of the cantilever. Non-contact mode eliminates lateral friction forces associated with contact mode, however a very fast controller must be used because it is very difficult to avoid attraction into the meniscus layer using this modality.

The desire to overcome the disadvantages associated with non-contact mode lead to the development of intermittent contact or "tapping" mode. Tapping mode still employs the adjustable z-controller to control the driving force of the oscillation, but now the tip is excited to greater amplitudes so that it intermittently comes into contact with the surface as it travels across the sample. The greater tip sample distance shifts the forces acting upon the cantilever into the coulombic repulsive regime, which increases oscillation frequency and thus the higher frequency oscillation compared to non-contact

Figure 11: A force vs. tip-sample distance curve showing the force regimes for the different operating modes.
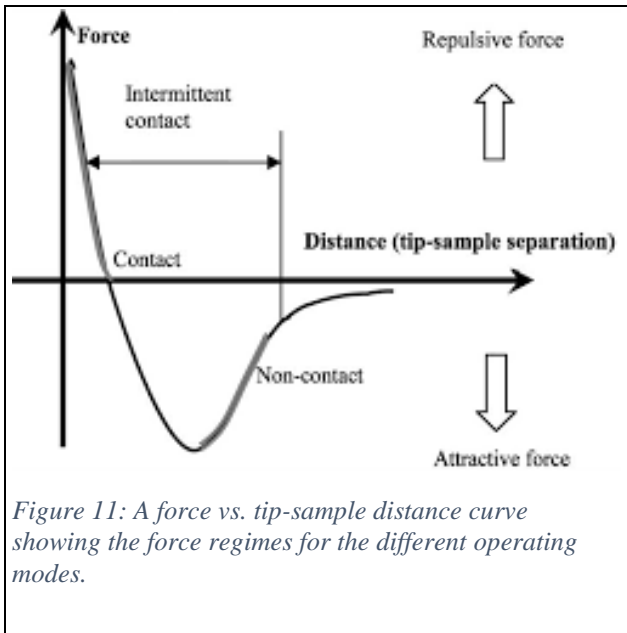
mode helps the tip to unstick quickly from the surface meniscus layer and to avoid lateral damage (L. Zitzler, 2002). This is because when the tip contacts the surface, it has sufficient oscillation amplitude to overcome the tip-sample adhesion forces, unlike contact and non-contact modes. A graphical representation of the force regimes based on tip-sample distance for the three modes of operation is presented in figure 11. We can see that that at

14

close tip-sample distances the repulsive force regime dominates, and conversely as the tip-sample distance increases the system moves into the attractive force regime (Paulo, 1999). Advantages of tapping mode include the fact that lateral forces are eliminated by restricting contact to the z-direction, and that the liquid meniscus trapping effect is overcome by high frequency oscillations. Some disadvantages of tapping mode are that scan speeds must be slightly slower due to the higher oscillation frequencies (5 minutes vs 2 minutes for a 3 um x 3 um image), and that because contact between the tip and the sample surface still occurs the tip can become dull and/or damaged over many uses (Chanmin Su, 2003).

Though contact and non-contact modes of operation are also possible, tapping mode has been chosen for use in our AFM actin imaging experiments due to its ability to resist the attractive meniscus forces that form on the sample surface in ambient environments and to reduce frictional forces on the tip which can distort imaging, produce artifacts, and damage both the tip and the sample. Figure 12 shows the Dimension 3100 AFM

Figure 12: The Dimension 3100 SPM System with NanoScope IV Controller

system used in this work, the procedure for its operation is found in the appendix.

2.4 Tip Convolution and Imaging Artifacts

This section will touch upon tip convolution and imaging artifacts in our atomic force microscopy studies. Tip convolution is an effect that is due to the radius of curvature of the tip being similar to or larger than the width of the features being imaged (D Tranchida, 2006). This creates inevitable artifacts in the image as the tip scans across the sample surface. This is because of a broadening effect which stretches the x and y dimensions of the image being displayed. This broadening effect of tip convolution is shown in figure 16. It is for this reason that the lateral resolution of AFM is much less reliable then the z resolution. Using the supplied probe tip geometry one can attempt to utilize deconvolution algorithms in software like SPIP or Gwyddion to correct for image distortions. Alternatively, the probe tip can be imaged with AFM and the geometry derived in order to run in a deconvolution algorithm (F. Atamny, 1995).

Other artifacts and distortions can arise when the tip is contaminated or dirty, or has been dulled over time from use. Artifacts can also be associated with increased noise

Figure 13: Illustration of the tip convolution effect in atomic force microscopy. Note the lateral widening effect of the artifact on the right. This is the source of the poor lateral resolution in AFM.
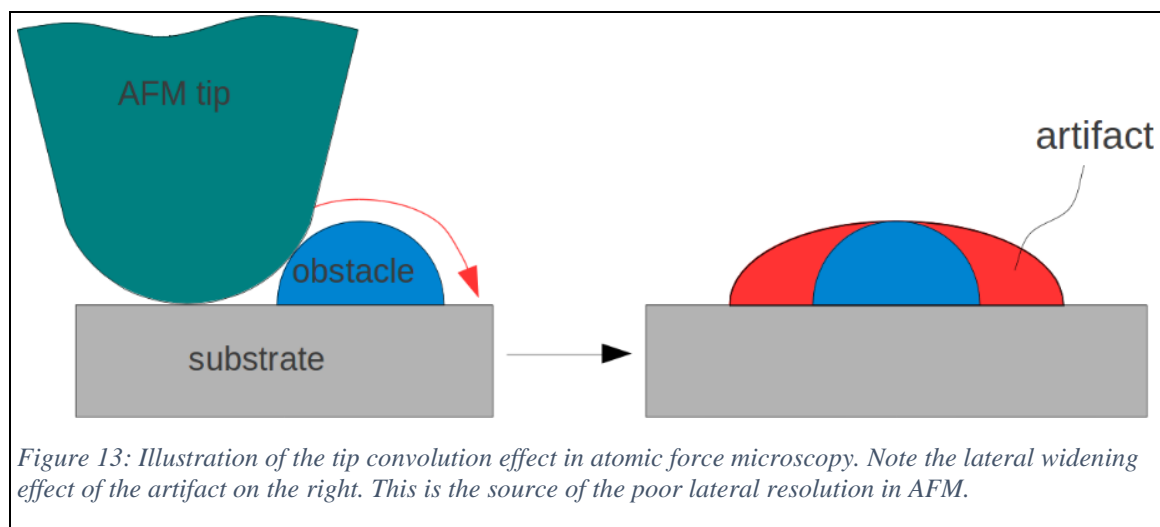
in the lab, or peculiarities or improper feedback in the z scanner. Another form of image distortion may arise if biomolecules have not properly adhered to the substrate surface and are experiencing motion during scanning. Due to the scale of imaging being conducted, atomic force microscopy is quite susceptible to various artifacts and image distortions which can make analysis difficult.

2.5 Actin Sample Preparation

This section details the sample preparation protocol developed for the single actin filament imaging studies. Preliminary studies were conducted by depositing 10 μl of each 1 μM and 5μM concentrations of F-actin onto glass slides, and capturing images using the AFM operation procedure outlined in the appendix. After being deposited onto the slide the samples were washed by pipetting 10 μl of water with into the sample, waiting for a few seconds, and then removing 10 μl of the 20 μl sample/water mixture with the pipette and disposing. This washing was repeated 6 times and pipetting was performed with smooth controlled motions. After the final wash approximately 10 μl of solution remained on the slide to dry. We prepared samples from a stock solution of 200 μM F-Actin diluted to the two different concentrations using a series dilution with F-actin buffer. A series dilution of 200 μM F-actin stock using F-Buffer was the procedure used to obtain the desired actin concentrations in all of the studies performed herein, although the glass slides were found to be too rough and/or easily contaminated to be used for nanoscale imaging of filaments.

Figure 14: Amanita Phalloides, the death cap mushroom. Phalloidin is one the seven toxins found in this mushroom.

The next studies conducted employed mica instead of glass, depositing 3 μl each of 5 μM and 20 μM concentrations of F-actin onto mica discs adhered to a glass slide with glue. The same washing procedure was observed as noted previously. These studies introduced the use of Phalloidin to the sample preparation, wherein Phalloidin is added to the actin samples in a 1:1 molar ratio for stabilization. Once the Phalloidin is added the samples should be allowed to sit for 30 minutes to an hour. This step was implemented in all of the imaging studies conducted.

Phalloidin is a phallotoxin (one of the seven toxins of the Amanita Phalloides or death cap mushroom shown in figure 14) which prevents depolymerization in F-actin, therefore disrupting the treadmilling effect by reducing

Figure 15: An F-actin trimer molecule with Phalloidin attached (red). This is the same site where an ATP molecule would attach.

monomer disassociation rates to zero (Coluccio, 1984). Adding Phalloidin to the F-actin samples should enable better imaging by eliminating loose G-actin monomers yielding longer strands of filament. Phalloidin is used currently for images of fixed samples, as the

toxin has been shown to stabilize actin in vivo and in vitro (Michael Melak, 2017) (Isegrády, 2004). A molecular dynamics image of Phalloidin attached to an f-actin molecule can be seen in figure 15. This is for developing a protocol of imaging, formation, and analysis; later an engineered gel would not be formed with Phalloidin as treadmilling would be desired for emergent function as previously discussed, as well as the fact that the toxin permeates cell membranes would not be biocompatible. In our case, Phalloidin is added to more easily image singular filaments by disrupting treadmilling, reducing excess G monomers and yielding longer filaments in samples

The next experiments we performed included a slight change in methodology inspired by an article that used AFM to observe F-actin on unstructured and nanostructured surfaces (Marina Naldi, 2009). The paper suggests that the best actin concentration at which to find individual filaments is at ~2.3 µM. The authors report further that they only found large aggregates of actin at higher concentrations tested, but

Figure 16: Target resolution/image quality for our AFM actin experiments, (Marina Naldi, 2009)
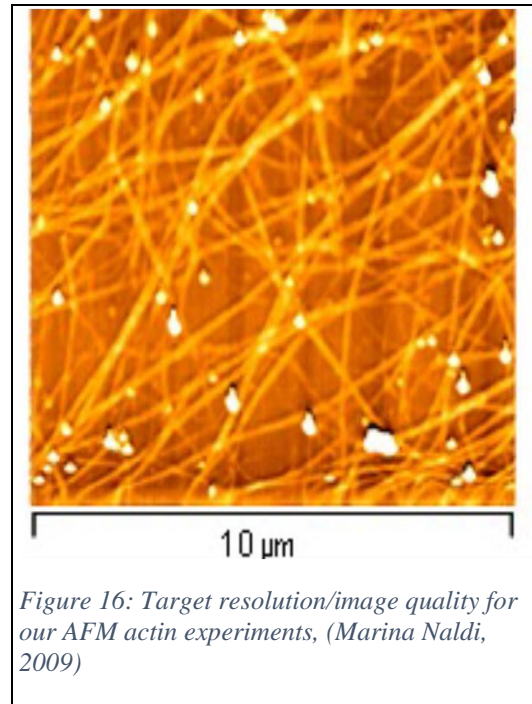
found no filaments at all below a concentration of 0.5 µM. Individual filaments were described as being more easily imaged further out from the center of the sample deposition point. Our laboratory used the results of this paper as a target for image quality, hoping to achieve the sort of resolution seen in figure 16. Additionally this paper inspired the use of

19

Magnesium Chloride ($MgCl_2$) in our sample preparation procedure. The use of $MgCl_2$ is an attempt to deposit positively charged magnesium ions between the natively negatively charged mica surface and the negatively charged actin, resulting in greater adsorption of actin onto the mica substrate surface. This greater adsorption is important to restrict the movement of biomolecules for stable imaging and to overcome the natural tendency for the actin to repel the similarly charged mica surface. For these experiments the mica surfaces were first freshly cleaved with a clean razorblade in order to use the less contaminated inner surface of the substrate. This methodology was adopted for the rest of the studies in this work as well. The cleaved mica discs were then adhered onto a glass slide using glue and set to dry. Once the glue was dry, the mica surfaces were treated with 20 μl of 100 mM $MgCl_2$. This proceeds to sit for ~10 minutes and then the mica surfaces are washed with water and allowed to dry before sample deposition. The actin concentrations tested under this regime were 0.5 μM, 1 μM, and 2 μM.

The final experimental methodology that we attempted for actin imaging was based on two selections from the literature (Hongda Wang, 2002) (Christian Pick, 2015), and did not use $MgCl_2$ to try to assist adsorption. The new procedure utilizes aminopropyltriethoxysilane (APTES) to covalently attach a charged amine group (*N*, *N*-diisopropylethylamine or DIPEA) to the mica substrates through vapor deposition in a desiccator that has been purged with nitrogen. These experiments used a series dilution from 200 μM to test actin concentrations of 1 μM, 2μM, 5μM, 10μM, and 20 μM. Mica was first freshly cleaved and adhered to glass slides as previously described. Then a desiccator is attached to a compressed nitrogen tank equipped with a pressure regulator and

allowed to purge the container of oxygen for several minutes. The desiccator is filled with nitrogen in order to purge oxygen out of the enclosed environment because the APTES and DIPEA compounds are very oxygen sensitive. After several minutes of purging insert the glass slides with mica adhered to them into the desiccator. Slow the flow of nitrogen slightly so that vaporized APTES and DIPEA are not later blown out of the container. Now insert a clean glass slide into the desiccator, quickly adding 30 µl of APTES and 10 µl of DIPEA (without letting the two mix) to the surface and closing the desiccator. Allow the nitrogen to purge for a minute or two at the lower rate and then seal the environment and remove the nitrogen tank. Now the APTES and DIPEA will vaporize and deposit onto the surfaces of the cleaved mica substrates. This should be left to deposit for at least two hours. After vapor deposition is complete, add 3 µl of each actin concentration to the prepared mica substrates. Let sit for ten minutes and then wash the deposits with water by pipetting 6 µl of water directly onto each 3 µl sample, and then waiting a few seconds and removing 6 µl from the sample/water mixture. This is repeated at least 6 times, and afterwards about 3 µl of solution should remain. The wash is performed to remove excess salts from the sample. Now the samples are left in the desiccator to dry before being imaged.

2.6 Actin-DNA Conjugation Procedure

The final set of experiments conducted by our lab for this work involved attempting to form actin-DNA conjugates and observe and measure them with the atomic force microscopy procedure developed earlier. To accomplish this, we combined two complementary DNA oligomers named sense and antisense separately with the cross-

linking molecule SMPB (succinimidyl 4-(p-maleimidophenyl) butyrate). SMPB binds

actin to DNA through its reactivity with amino groups and sulfhydryl groups. After the two oligomers were modified with the crosslinkers they were conjugated with actin. This process is shown in Figure 17. The actin-DNA complexes were diluted with unmodified actin in different proportions (1:5, 1:25, and 1:100), and then mixed for AFM studies. What follows is the step by step procedure for this experiment:

Figure 17: A) depiction of F-actin/DNA conjugates that have been crosslinked by SMPB, the gray spheres are the G monomers that make up the F-actin filaments, the protruding black lines are the sense and antisense DNA oligomers. B) The complex formed after mixing the sense and antisense conjugates from A.
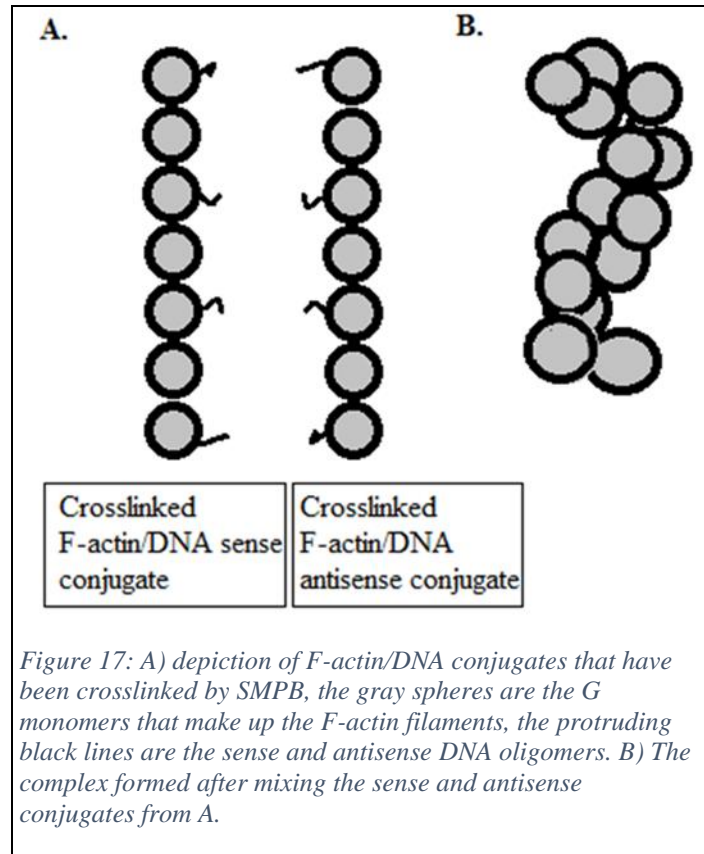
1. Prepare a stock solution of DNA oligomers (sense and antisense) in buffer, the buffer is as follows: 100mM Na phosphate, 150 mM NaCl, 1mM EDTA, pH 7.5. For DNA sense: add 501 μL of buffer, which makes 100 μM DNA stock. For DNA antisense: add 676 μL of buffer, which makes 100uM DNA stock. The buffer should be added to the DNA, put in the vortex mixer, allow to sit for 5 min, vortex mixed again. Take 196uL each DNA stock for conjugation and place the leftovers in -20C.

22

2. Prepare the stock solution of cross-linkers (SMPB or succinimidyl 4-p-maleimidophenyl butyrate). SMPB is an unfriendly chemical which cannot be stored and is moisture sensitive. Solution preparation and subsequent adding to DNA must be done quickly. Equilibrate the vial to room temperature before opening to avoid moisture condensation inside of the container. Weigh out 5 mg of SMPB and dissolve in DMF (dimethylformamide) to 50 mM. Dissolve reagent and use immediately before hydrolysis occurs.

3. Add 4 μl of prepared 20 mM SMPB solution to 196 μl of sense DNA stock.

4. Add 4 μl of prepared 20mM SMPB solution to 196 μl of antisense DNA stock.

5. Discard prepared SMBP solution.

6. This will create two DNA conjugates which will be worked on in parallel.

7. Incubate mixtures for two hours at room temperature, total volume 200 μl each, 1:10 DNA:SMPB.

8. Use a small spin concentrator with the cutoff at 3 kDa to wash the DNA from the excess of SMPB. Add 200 μl of Sodium Phosphate buffer to the DNA-SMPB mixture and spin at 14k until a volume of 200 μl is reached, repeating this 10 times. Switch to F-buffer for the last five washes. This will dilute the non-reacted SMPB solution ~1000 fold. Spin to a final volume of 200 μl, and collect the washed DNA in a fresh spin concentrator tube.

9. Measure the concentration of washed DNA by running a spectrum analysis between 250 nm and 500 nm. Use F-buffer as a blank and save spectrum data.

10. Mix 200 μl of 20 μM F-actin and 200 μl of 100 μM conjugated DNA-SMPB solution. Incubate them for two hours at room temperature then leave them overnight on ice.

11. Use a spin concentrator with cutoff at 30 kDa to wash actin from the excess of DNA. First, spin to a volume of 200 μl and collect the flow through. Then add 200 μl of F-buffer to the column and spin to 200 μl again. Collect the flow through and repeat. Measure the absorption spectra of all three flow-throughs, wavelength range 250 nm to 500 nm, using F-buffer as a blank. Continue to wash actin, repeating to a total of ten washes. The final volume should be 200 μl of labelled F-actin. Save the measured samples.

12. Use a new spin concentrator with cutoff 3 kDa for F to G-buffer exchange. The same technique is used, 200 μl of sample is added to 200 μl of G-buffer and spun 7-10 times. At this point there will be two samples of G-actin labelled with sense and antisense DNA, at a volume of 200 μl concentrated to 20 μM.

13. Make mixes of labelled to unlabeled actin at concentrations 1:5, 1:25, and 1:100. For the 1:5 mix take 10 μl of labelled 20 μM actin and 40 μl of unlabeled 20 μM actin. For the 1:25 mix take 10 μl of 1:5 mix and 40 μl of unlabeled 20 μM actin. For the 1:100 mix use 10 μl of 1:25 mix and add 30 μl of 20 μM actin. Add salts to a final concentration of 50 mM Potassium Chloride and 2 mM Magnesium Chloride. The final volume of each sample should be ~80 μl at an actin concentration of 10 μM. Let the samples polymerize overnight at 4 degrees Celsius. There should be a total of six samples.

14. Use a spin concentrator with 30 kDa cutoff for a buffer exchange to F-buffer. Add 320 μl of F-buffer in each spin concentrator and add 80 μl of sample. Spin to a volume of 200 μl, add 200 μl of F-buffer and spin again. Repeat this seven times. Concentrate to a final volume of 100 μl. The concentration of actin in these samples will be about 8 μM.

15. Add 1 μl of Phalloidin to each sample and incubate for one hour at room temperature.

16. Take 10 μl of each sample and dilute them four times by adding 30 μl of F-buffer to each. The actin concentration will now be 2 μM. Save the rest on ice.

17. Mix the obtained 40 μl sense and antisense samples. There should be three mixes, each ~80 μl.

18. Prepare mica substrates with APTES and DIPEA, depositing 3 μl of each of three mixes and one of the six unmixed samples as a control, diluting it to 2 μM. Store leftovers on ice and wait 10 mins.

19. Use pipette wash procedure, adding 6 μl to each sample, waiting a few seconds, then removing 6 μl of sample and discard. This is done ~6 times.

20. Dry the samples and run an AFM study.

The final experiment we conducted repeated the actin/DNA sense and antisense conjugation study and added two new aspects: the introduction of gelsolin to modify the samples, and the experimental formation of a G-actin based DNA molecule.

Figure 18: An illustration of G-actin monomers connected by complimentary DNA oligomers forming a dumbbell-shaped structure. Protruding black lines represent the DNA oligomers.
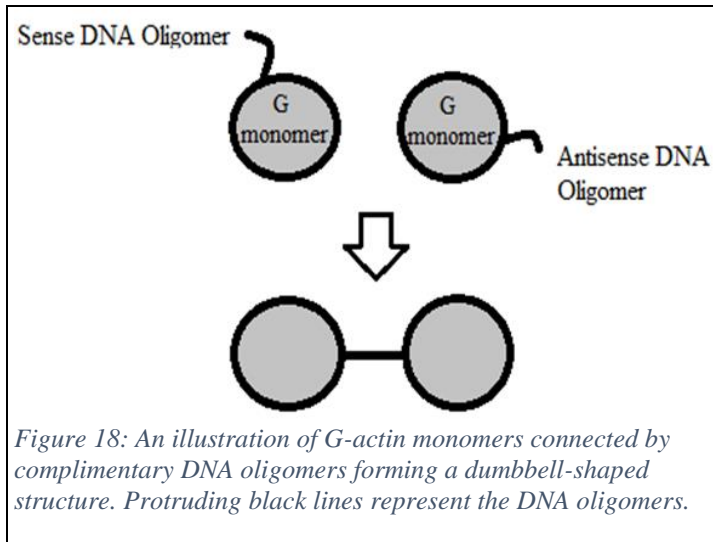
Gelsolin has been shown to sever and cap F-actin filaments for imaging studies (Taiji Ikawa, 2007). This sectioning action controls the length of actin filaments and may help to visualize interactions without other filaments getting in the way. In addition the structure of actin and gelsolin can change when combined (JKwiatkowski, 1999) and could yield interesting molecular configurations when cross-linked with DNA.

The experimental formation of a G-actin DNA molecule is based on the idea that G-actin monomers which have been labelled with sense and antisense DNA oligomers might form structures that resemble dumbbells, with spherical G-actin monomers connected by the complementary DNA strands (Figure 18). When added to unlabeled actin, the dumbbells would act as a nucleator for crosslinked actin filaments. The following was the procedure for conducting this final study:

1. Prepare a stock solution SMPB. Equilibrate the vial to room temperature before opening to avoid moisture condensation inside of the container. Weigh out 5 mg of SMPB and dissolve in DMF (dimethylformamide) to 50 mM. Dissolve reagent and use immediately before hydrolysis occurs.

2. Take 98 µl of each DNA oligomer stock for conjugation.

3. Add 2 μl of prepared 50 mM SMPB solution to 98 μl of YNs1 DNA stock and mix well. This makes a 1:10 DNA: SMPB labelling ratio.

4. Add 2 μl of prepared 50 mM SMPB solution to 98 μl of YNas1 DNA stock and mix well.

5. Discard the prepared SMPB solution.

6. This will make two DNA conjugates which will be worked on in parallel.

7. Incubate the mixtures for two hours at room temperature. They should have a volume of 100 μl each and be at a 1:10 DNA: SMPB ratio.

8. Use a small spin concentrator with the cutoff at 3 kDa to wash the DNA from the excess of SMPB. Add 300 μl of Sodium Phosphate buffer to the DNA-SMPB mixture and spin at 14k until a volume of 100 μl is reached, repeating this 6 times. Switch to F-buffer for the last three washes. This will dilute the non-reacted SMPB solution ~1000 fold. Spin to a final volume of 200 μl, and collect the washed DNA in a fresh spin concentrator tube. This will be 200 μl of 50 μM DNA conjugated with the SMPB linker.

9. Measure the concentration of washed DNA by running a spectrum analysis between 250 nm and 500 nm, using F-buffer as a blank. Save the spectrums.

10. Mix 200 μl of 10 μM F-actin with 200 μl of conjugated DNA-SMPB solution. Incubate for two hours and then leave overnight on ice.

11. Use a small spin concentrator (cutoff 30kDa) to wash the actin from the excess of DNA. First spin to a volume of 200 μl and collect the flow through. Then add 200 μl of F-buffer to the column and spin to 200 μl again, collecting the flow through.

Repeat once more. Measure the absorption spectra of all three flow throughs, using F-buffer as a blank. Continue to wash the actin, repeating to a total of 10 washes. The final volume should be 200 μl of labeled F-actin at a concentration of 10 μM.

12. Use a new spin concentrator with a cutoff of 3kDa for F-buffer to G-buffer exchange. Add 200 μl of sample to 200 μl G-buffer and spin for 7 – 10 repetitions. At this point you should have two samples of G-actin labeled with the sense and antisense DNA at a final volume of 200 μl, and a concentration of 10 μM. Leave the samples for two hours at room temperature to equilibrate. Spin in a small centrifuge for 6 hours at a temperature of 4 degrees Celsius at maximum speed. Carefully collect the supernatant. Do not disturb the pellet, even if it is not visible. This is labeled G actin.

13. Measure the absorption spectra between 250 nm and 500 nm using G-buffer as a blank. Save the sample.

14. Measure the absorption spectrum of the unlabeled 10 μM G-actin at 250 nm-500nm, using G-buffer as a blank.

15. Compare the spectra of labeled and unlabeled actin. If the hump at 290 nm looks the same, the concentration is the same. If the hump at 290 nm is different for labeled and unlabeled actin, the volume of labeled actin should be adjusted for following mixes to have a controlled mix of 1:5 and 1:25.

16. Take 50 μl of each sample of labeled G actin and mix them together. Leave them for two hours at room temperature for DNA to form a duplex. This will form the G-actin dumbbell solution at a volume of 100uL and a concentration of 10uM.

17. Make mixes of labeled to unlabeled G-actin at ratios of 1:5 and 1:25, for the following three samples: actin-sense DNA, actin-antisense DNA, actin dumbbells. For the 1:5 mix take 20 μl of DNA-labeled G actin at 10 μM and add 80 μl of unlabeled G actin at 10 μM. For the 1:25 mix take 20 μl of the 1:5 mix and add 80 μl of unlabeled actin at 10 μM. Add Potassium Chloride and Magnesium Chloride salts to a final concentration of 50 mM for KCl and 2 mM for $MgCl_2$. The final volume of the 1:5 sample is 80 μl with an actin concentration of 10 μM. The final volume of the 1:25 sample is 100 μl with an actin concentration of 10 μM. Polymerize overnight at 4 degrees Celsius. There should be a total of six samples: two sense and two antisense actin-DNA conjugates, as well as actin dumbbells diluted with unlabeled actin.

18. Use a 30 kDa spin concentrator for buffer exchange to F-buffer. Add 320 μl of F-buffer in each spin concentrator and 80 μl of sample. Spin to a volume of 200 μl, then add 200 μl of F-buffer and spin again. Repeat this 7 times. Concentrate to a final volume of about 100 μl. The concentration of actin in these samples should be about 8 μM.

19. Prepare 100 μl of unlabeled 8 μM F-actin.

20. Add Phalloidin to each actin sample. Incubate all of the samples for 1 hour at room temperature.

21. Prepare the gelsolin solution. The stock solution is 6.6 μM. Prepare a 100x diluted solution by combining 990 μl of F-buffer and 10 μl of the gelsolin stock solution.

22. Add gelsolin to each actin sample at a ratio of 1:100 gelsolin to actin. Take 20 μl of actin sample and add 100 μM $CaCl_2$ (8uL at 1 mM $CaCl_2$), add 24 μl of diluted gelsolin, and then add F-buffer to a volume of 80 μl.

23. Mix 40 μl of each of the sense and antisense samples. Incubate the mixture for two hours at room temperature for the DNA to form a duplex. There should be four mixes: 1:5 and 1:25, with and without gelsolin, each at a volume of about 80 μl.

24. The following samples are expected to be prepared:

    1) Actin DNA sense:antisense mix 1:5

    2) Actin DNA sense:antisense mix 1:5, 1:100 gelsolin

    3) Actin DNA sense:antisense mix 1:25

    4) Actin DNA sense:antisense mix 1:25, 1:100 gelsolin

    5) Actin DNA dumbbells mix 1:5

    6) Actin DNA dumbbells mix 1:5, 1:100 gelsolin

    7) Actin DNA dumbbells mix 1:25

    8) Actin DNA dumbbells mix 1:25, 1:100 gelsolin

    9) Actin DNA 1:5 sense sample,

    10) Actin DNA 1:25 sense sample,

    11) Unlabeled F actin, 2uM

    12) Unlabeled F actin, 2uM, 1:100 gelsolin

25. Prepare mica substrate with APTES and DIPEA, depositing 3 μl of each of the prepared samples. Let the samples sit for 10 minutes.

26. Wash each of the sample using the aforementioned pipetting technique. Wash with 6 μl of water 6-7 times.

27. Let the samples dry and run the AFM for imaging.

CHAPTER 3. RESULTS/DISCUSSION

3.1 Actin Study Results

The purpose of these studies was to develop a protocol of sample preparation for

the visualization of single actin filaments at the nanoscale for future studies of novel
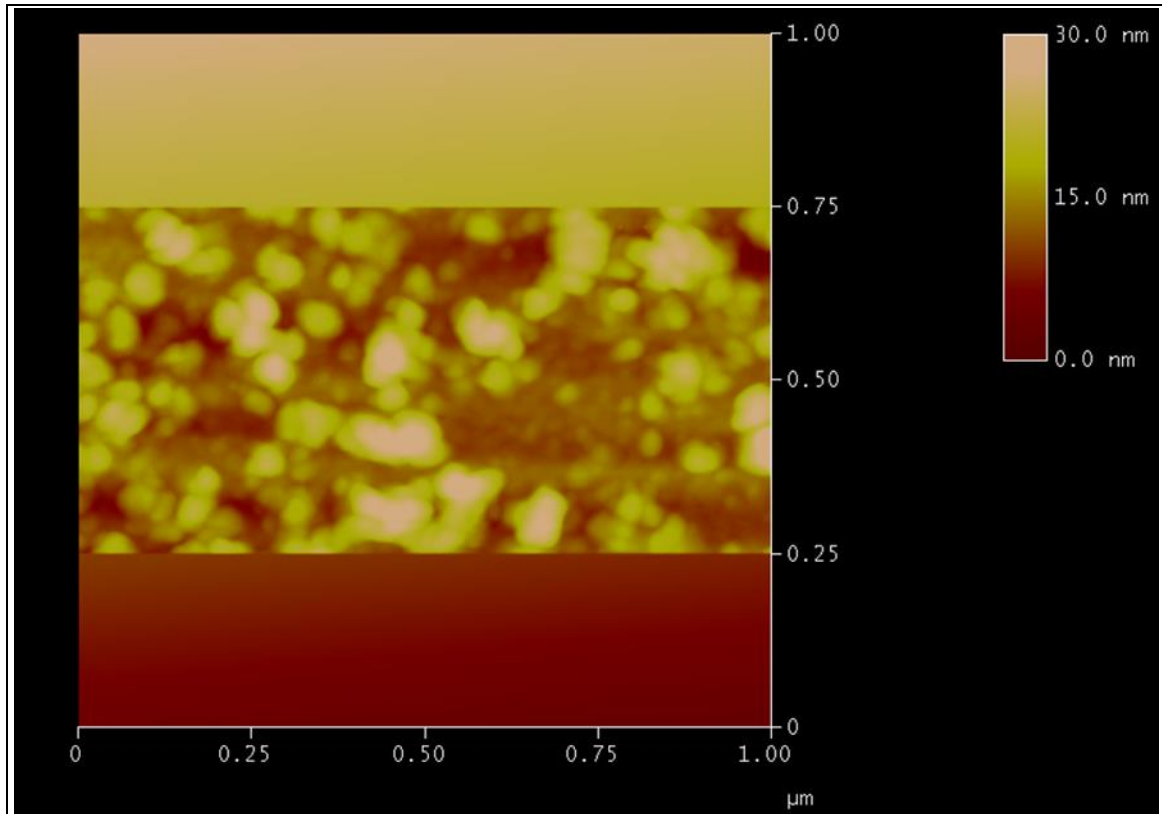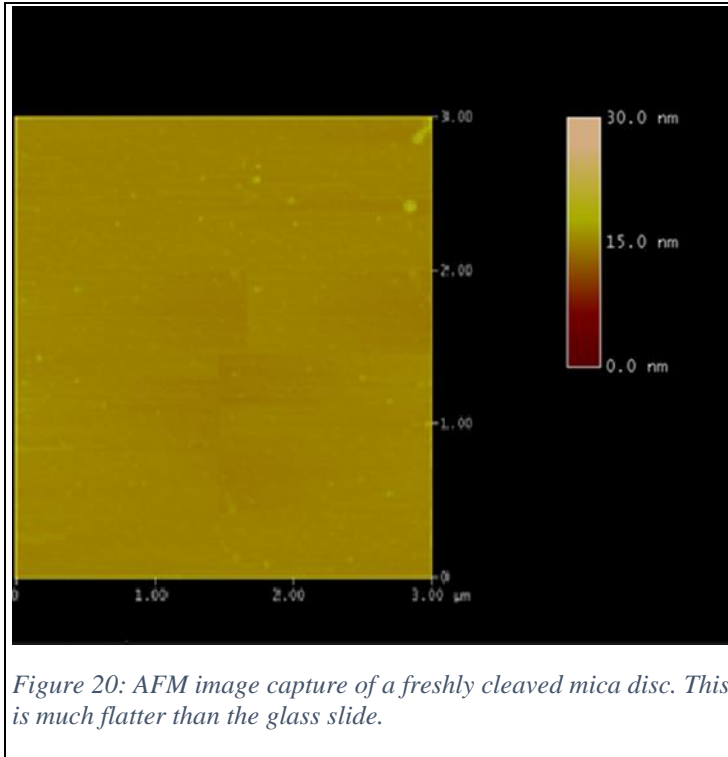

Figure 19: AFM image taken of a clean glass slide. Features on the slide are larger than actin diameters based on the z-direction color scale and therefore would obfuscate any filament images.

engineered actin/DNA hydrogels. Preliminary studies were conducted by depositing 10 μl

of each 1 μM and 5μM concentrations of F-actin onto glass slides, and capturing images

using the AFM operation procedure described in the appendix.

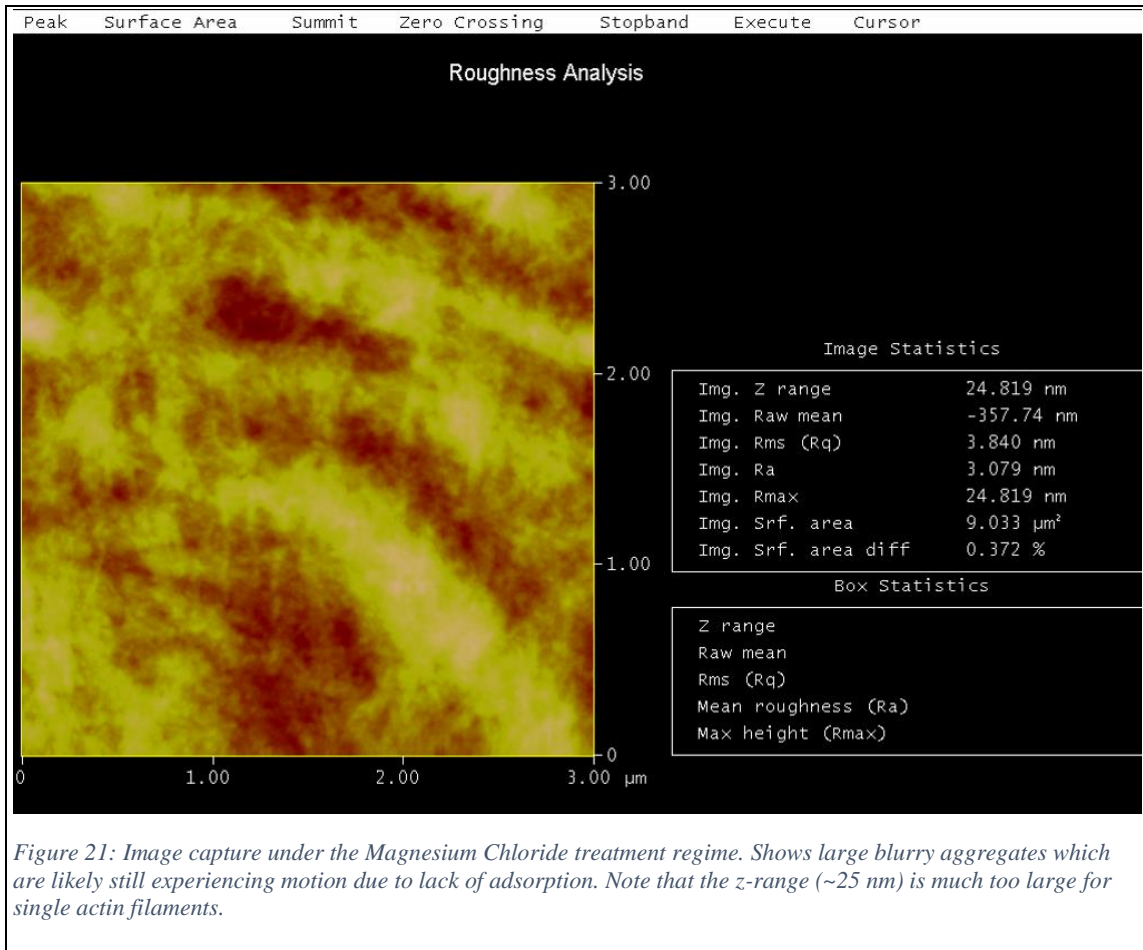*Figure 20: AFM image capture of a freshly cleaved mica disc. This is much flatter than the glass slide.*

These experiments revealed that untreated glass cover slides were too rough and/or easily contaminated for functional actin resolution at the size scales used, as features on the AFM glass slide image were much larger than actin filament diameters, with some features measuring over 30 nm tall, and would obscure their imaging (figure 19). Switching to freshly cleaved mica discs as a substrate revealed AFM images which were much more uniform (figure 20). The average change in z-distance across the cleaved mica was measured to be about 0.3 nm, which would allow single filaments to be visible. Despite the change in substrate however, filaments could not be observed due to problems with sample motion resulting from a failure to stabilize the protein on the substrate.

At this point we began the procedure of treating the mica surface with 20 μl of 100 mM $MgCl_2$, using actin concentrations of 0.5 μM, 1 μM, and 2 μM, and searching further from the deposition point to find individual filaments. Though we would choose to keep actin concentration near 2 μM for the rest of the studies and also continued to look for single filaments farther from the deposition point, it was determined that

33

treatment of the mica surface with $MgCl_2$ was not effective in the immobilization of actin

on the substrate. Scans performed under this regime show large blurry aggregates which

appear to be adhered but experiencing motion and causing distortions in the captured

images. All of the scans conducted using the $MgCl_2$ treatment procedure resulted in the

Figure 21: Image capture under the Magnesium Chloride treatment regime. Shows large blurry aggregates which are likely still experiencing motion due to lack of adsorption. Note that the z-range (~25 nm) is much too large for single actin filaments.

same type of unresolved image as shown in figure 21.

Using the tip geometry we attempted to use deconvolution algorithms in SPIP and

Gwyddion to correct for distortions, but the deconvolution had no effect on the images,

confirming that the images observed were in fact real and not artifacts. This realization

34

led to the implantation of a new methodology for actin adsorption in the form of the
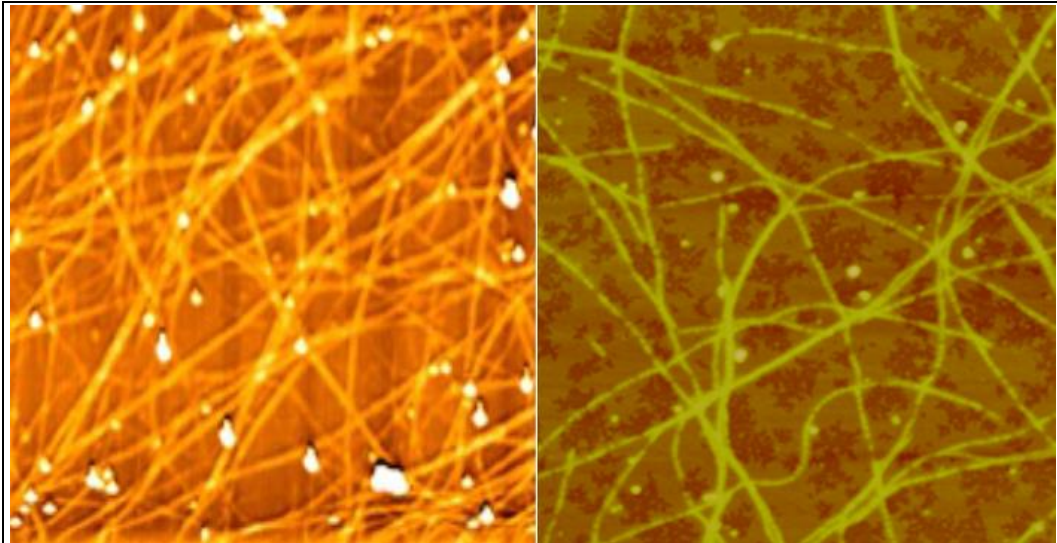
previously mentioned vapor deposition technique.

Figure 22: A comparison of the target image (left) and an actual retrieved image (right) using the vapor deposition method. The dimensions on the left are 10 um x 10 um, on the right they are 3 um x 3 um

The new procedure utilized aminopropyltriethoxysilane (APTES) to covalently

attach a charged amine (*N*, *N*-diisopropylethylamine) to the mica substrates through

vapor deposition in a desiccator purged with nitrogen. This method has been successful in

the nanoscale resolution of actin filaments at concentrations of 5uM, 2uM, and 1uM, with

large aggregates of filaments found at higher concentrations. When matched with the

initial target image presented earlier, the retrieved actin images compare quite favorably

(as can be seen in figure 22). The images were further analyzed and measurements of

filament diameters and approximate persistence lengths were recorded using the section

function in the Nanoscope 5.31 software. Persistence length is a measure of flexibility in

a biopolymer, related to the length it can be treated as a stiff segment before changing

angles (bending). To measure the persistence lengths, the section function in the software

35

was used to trace and measure observed rigid length segments in the filaments.

Measurements were made between points of the filament which showed no observable

change in direction. The values of the segments were tabulated and averaged for each

sample concentration. The average filament diameter across all F-actin images was found

to be about 6.2 nm. This corresponds to measurements of F-actin diameters in the

literature (Cooper, 2000). The average persistence length under this protocol was found

to be about 0.8 μm. The protocol developed in this study was thus found sufficient for the

characterization of individual F-actin filaments, and was deemed to be suitable for the

imaging of the potential actin/DNA hydrogel molecules in the conjugation studies in the

next section and for planned future experiments.

3.2 Actin/DNA Conjugation Study Results

Table 1: Average filament diameters and persistence lengths compared between Actin/DNA conjugation samples, the F-actin control, and previous F-actin samples.

Labelled to Unlabeled Concentration	Average Filament Diameter (nm)	Average Persistence Length (um)
1:5	2.03 +/- 0.83	0.100 +/- 0.024
1:25	5.56 +/- 1.60	0.550 +/- 0.220
1:100	4.83 +/- 0.53	0.670 +/- 0.182
Unlabeled F-actin Sample	4.04 +/- 1.15	0.750 +/- 0.190
Average of Previous Actin Samples	6.13 +/- 1.37	0.800 +/- 0.201

In the first Actin/DNA conjugation experiment we combined two complementary

DNA oligomers called sense (YNs1) and antisense (YNas1) separately with cross-linking

molecules, and then attached the separate mixtures to actin in concentrations of 1:5, 1:25,

and 1:100 labeled to unlabeled actin. Finally the two solutions (DNA YNs1 with cross-

linkers and actin, and DNA YNas1 with cross-linkers and actin) were mixed together at each concentration for conjugation.

Table 1 shows average filament diameters and persistence lengths of the three DNA/actin conjugation samples compared with the averages of the F-actin samples. Concentration of labeled to unlabeled actin was shown to cause changes in average filament diameter and persistence length. The measured filament diameters of the conjugates are lower on
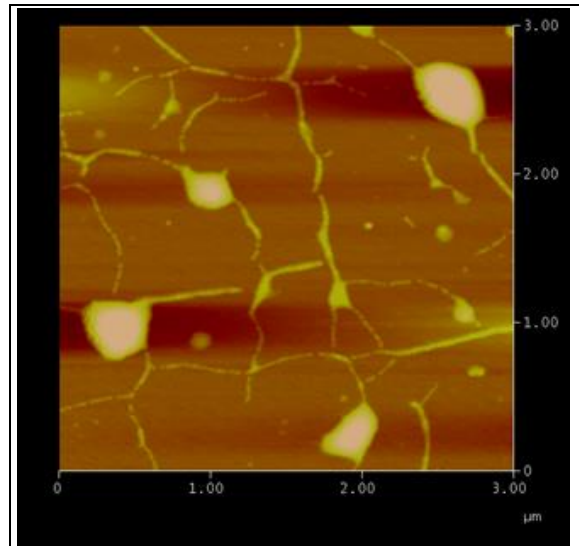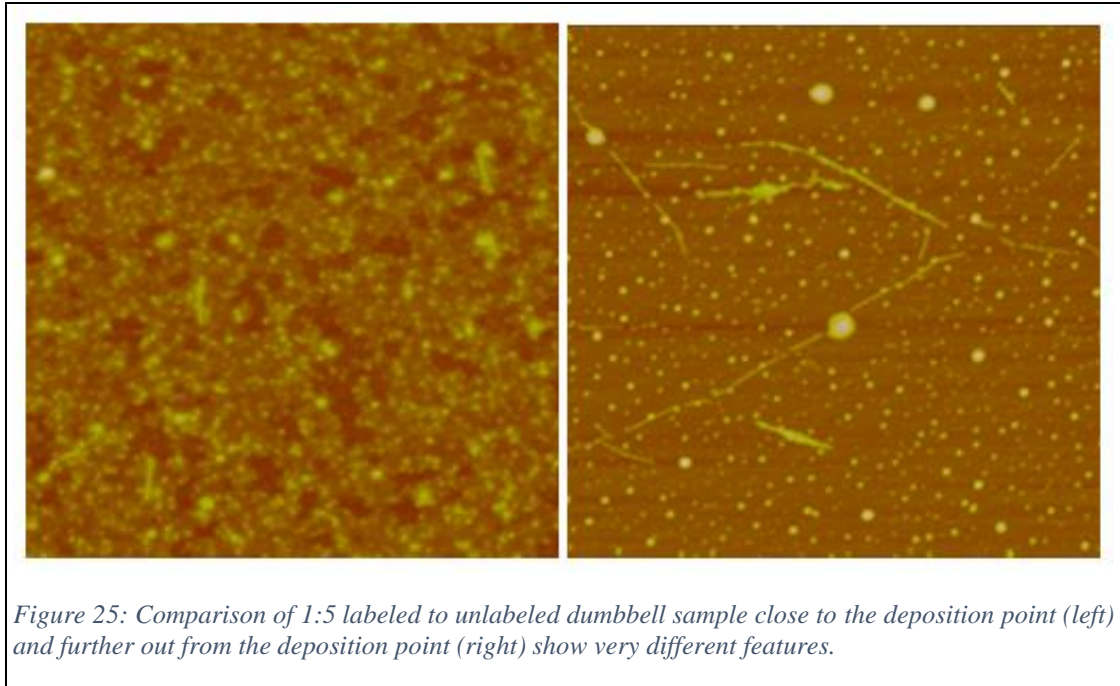

Figure 23: 2 μM unlabeled F-actin sample image from the first conjugation study.

average than the plain actin filaments. Additionally the persistence lengths of the actin filaments were shown to be much longer than the persistence lengths of the actin/DNA conjugates, with average actin filament persistence lengths measuring 0.75 um +/- 0.19 um, compared to 0.10 um +/- 0.83 um, 0.55um +/- 0.22 um, and 0.67 um +/- 0.18 um for the 1:5, 1:25, and 1:100 concentration conjugates respectively. The 2 μm F-actin control sample for the study is shown in figure 23, and the images of the actin/DNA conjugation samples of each concentration are displayed in figure 24. After this initial conjugation study our lab performed an exploratory study as a precursor to our final experiment based on the idea that G-actin monomers which have been labelled with sense and antisense DNA oligomers might form structures that resemble dumbbells, with spherical G-actin monomers connected by the complementary DNA strands.

Figure 24: Actin/DNA conjugate images. Sense to Antisense concentrations of 1:5 (top), 1:25 (middle) and 1:100 (bottom)
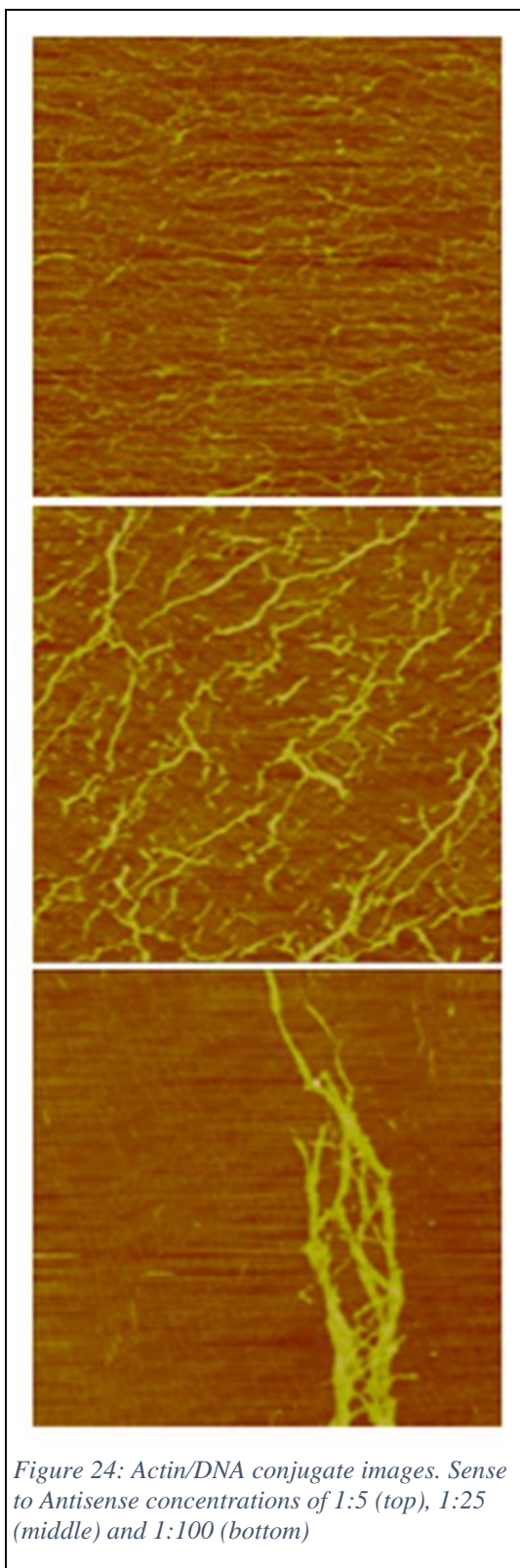
In this study, the dumbbells are first formed, and then diluted in unlabeled actin to form filaments which are already crosslinked. The first conjugate study on the other hand relies on combining actin with DNA, diluting it with unlabeled actin, forming filaments and mixing sense and antisense mixture to form a gel. The same labeled to unlabeled concentrations were studied as in the previous conjugation study, 1:5, 1:25, and 1:100.

The 1:5 concentration sample (figure 25) showed different features when imaged closer to and farther out from the deposition point, with the former displaying a more compact structure with average height around 3.3 nm +/- 1 nm, and the latter showing filamentous structures with an average diameter around 4.3 nm +/- 0.65 nm with a persistence length of about 720 nm +/- 79 nm. The image further from the deposition point also reveals spherical objects which average ~9.7 nm +/- 0.83 nm in height. The 1:25

Figure 25: Comparison of 1:5 labeled to unlabeled dumbbell sample close to the deposition point (left) and further out from the deposition point (right) show very different features.

sample seen in figure 26 showed long filamentous structures which appeared bundled together with branching filaments extending outwards. The average diameter was recorded at ~3.8 nm +/- 0.8 nm and the measured persistence length was around 712 nm +/- 270 nm. The 1:100 concentration dumbbell sample pictured in figure 27 showed filamentous looking structures which had average diameters of 3.2 nm +/- 0.6 nm, but the persistence length varied depending on how close to the deposition point the sample was viewed (from ~692 nm +/- 100 nm close to deposition to 267 nm +/- 28 nm further out).

Table 2 compiles the measurements for each DNA/actin dumbbell sample. Again we see changes in average structure height and
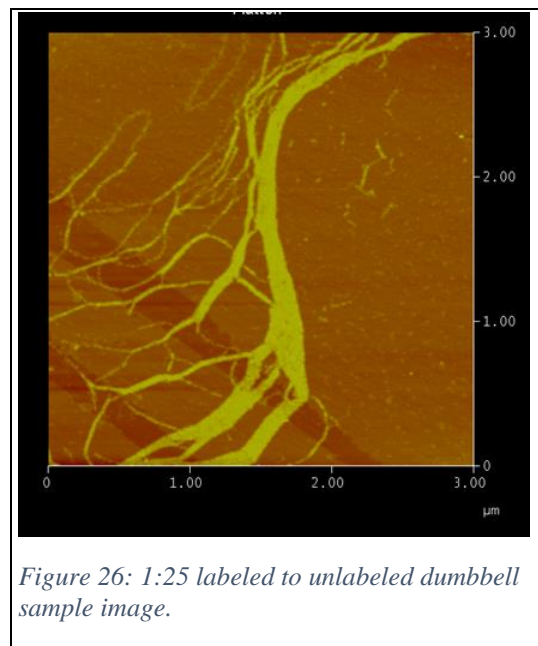

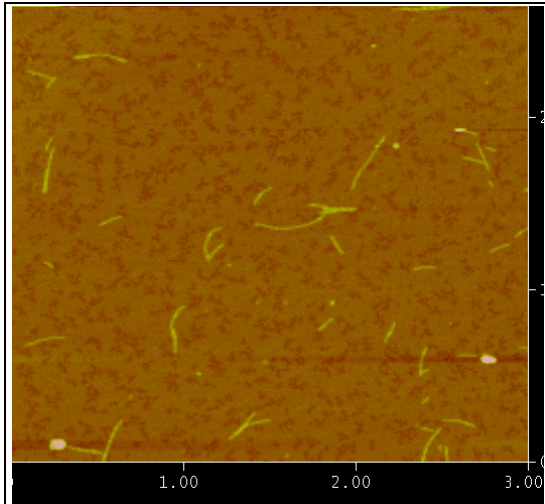*Figure 26: 1:25 labeled to unlabeled dumbbell sample image.*

39

Figure 27: Image of the 1:100 concentration dumbbell sample.

average persistence length based on concentration of labeled to unlabeled actin. The final experiment performed by our laboratory attempted to repeat both the F-actin/DNA conjugation study and the G-actin dumbbell investigation, while introducing gelsolin to modify the samples by severing and capping actin filaments. There were many difficulties in the course of the final conjugation procedure.

Table 2: A table comparing the DNA/actin dumbbell samples for average height and persistence length. When distance from the deposition point has caused feature changes it is denoted as close or far.

Labelled to Unlabeled Concentration	Average Structure Height (nm)	Average Persistence Length (nm)
1:5	Close: 3.3 +/- 1.0 Far: 4.3 +/- 0.65	Close: n/a Far: 720 +/- 79
1:25	3.8 +/- 0.80	712 +/- 270
1:100	3.2 +/- 0.60	Close: 692 +/- 100 Far: 267 +/- 28

According to the absorption spectra collected, the antisense sample contained seven times less DNA than the sense sample. Since 1:5 and 1:25 mixes were made for each sample, and the data suggested that antisense 1:5 is close to sense 1:25, work on sense 1:5 and antisense 1:25 was stopped and it was decided to focus on just the sense 1:25 and antisense 1:5 mix, with and without gelsolin added. Assuming the 7x difference in the DNA content in these samples there would be a sense 1:25 - antisense 1:35 mix.

Additionally there were problems with several of the samples. The 2 μm F-actin samples with and without gelsolin produced distorted unreal images. Three of the dumbbell samples also produced distorted images although it looked to be the cause of potential motion on the substrate similar to the early Magnesium Chloride studies. The 1:5 labeled to unlabeled sample was the only dumbbell sample
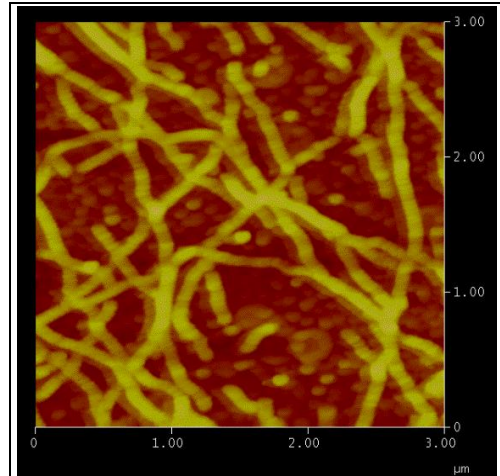

Figure 28: The 1:5 concentration dumbbell sample.

to produce an image (figure 28). The image featured filamentous structures which had an average height of 4.47 nm +/- 1 nm and persistence lengths of about 615 nm +/- 70 nm. The sense 1:25 and antisense 1:5 mix with and without gelsolin also produced several resolved images. The mixture without gelsolin (figure 29) showed filaments that had an
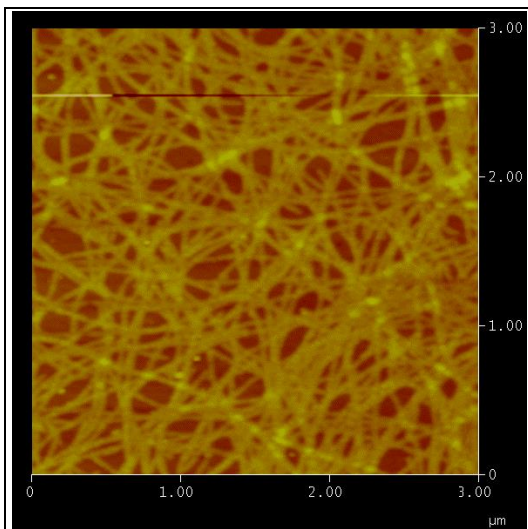

Figure 29: The sense 1:25 antisense 1:5 mixture without gelsolin.

average diameter of ~ 4.13 nm +/- 0.6 nm and an average persistence length of 560 nm +/- 90 nm. The mixture with gelsolin added (figure 30) produced filaments with an average diameter of ~6.6 nm +/- 1 nm and an average persistence length of ~1.853 μm +/- 0.9 μm. The mixture with gelsolin also showed an abundance of unidentified spherical objects which had an average height

41

~7.8 nm +/- 0.92 nm. Standard deviations were collected from 20 data points for each measurement.

To conclude, a reliable protocol of sample preparation for the visualization of single actin filaments at the nanoscale has been developed which makes future DNA/actin hydrogel conjugation studies possible.
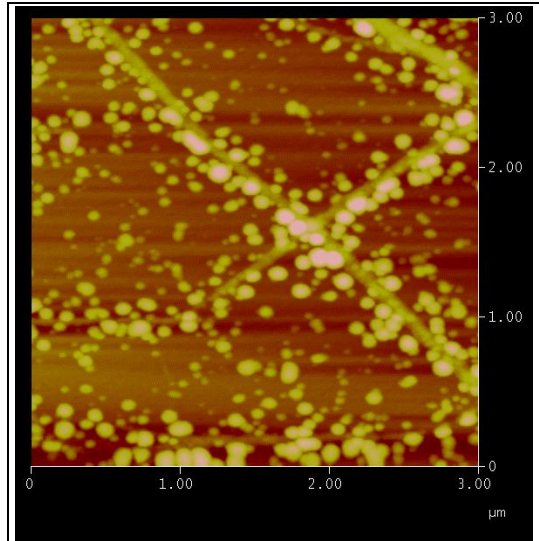

Figure 30: The sense 1:25 antisense 1:5 mixture with gelsolin added.

CHAPTER 4 CONCLUSION

The purpose of this work was to develop a protocol of sample preparation for the visualization of single actin filaments at the nanoscale for future studies of engineered DNA/actin hydrogels using atomic force microscopy. A procedure was developed which utilized aminopropyltriethoxysilane (APTES) to covalently attach a charged amine group (*N*, *N*-diisopropylethylamine) to mica substrates through vapor deposition in a desiccator that had been purged with nitrogen before deposition of F-actin samples and imaging with AFM. This method reliably produced images of individual actin filaments suitable for studies of engineered actin hydrogels.

In addition, initial work was begun on the formation of two different potential DNA/actin conjugate complexes, both using complementary DNA oligomers (sense and antisense) combined with crosslinking molecules (SMPB) to actin. One of them is an F-actin DNA conjugate, and the other is a dumbbell shaped G-actin complex. Initial data analysis has shown differences in average filament diameter and average persistence lengths in conjugate samples compared to actin samples, as well as a possible relationship between those metrics and the concentration of labeled to unlabeled actin in each sample.

F-actin and DNA have both been shown to exhibit potential for use in biocompatible engineered hydrogel applications. This work has developed a protocol of sample preparation for the nanoscale visualization of two novel engineered DNA/actin complexes based on AFM studies of filamentous actin and began preliminary studies into their development.

REFERENCES

A. Ott, M. M. (1993). Measurement of the persistence length of polymerized actin using fluorescence microscopy. *Physical Review E*, 1642.

Akihiro Narita, E. U. (2016). Direct observation of the actin filament by tip-scan atomic force microscopy. *Microscopy*, 370-377.

Blancaflor, Y.-S. W. (2004). Green fluorescent protein fusions to Arabidopsis fimbrin 1 for spatio-temporal imaging of F-actin dynamics in roots. *Cytoskeleton*, 79-93.

Brittanica (2018, Dec 10). *DNA: chemical compound*. Retrieved from Brittanica Encyclopedia online: https://www.britannica.com/science/DNA

Bruker. (2010, January 9). *TappingMode AFM*. Retrieved from Nanostructure Physics: http://www.nanophys.kth.se/nanophys/facilities/nfl/afm/fast-scan/bruker-help/Content/TappingMode%20AFM/TappingMode%20AFM.htm

Bruker. (2019, January 7). *Scanning Probe Microscopes*. Retrieved from Bruker: https://www.bruker.com/products/surface-and-dimensional-analysis/atomic-force-microscopes/campaigns/spm-microscopes-intro-to-scanning-probe-microscopy.html

Changjin Huang, D. Q. (2018). Controlled molecular self-assembly of complex three-dimensional structures in soft materials. *PNAS*, 70-74.

Chanmin Su, L. H. (2003). Studies of tip wear processes in tapping mode™ atomic force microscopy. *Ultramicroscopy*, 135-144.

Christian Pick, C. A. (2015). Micropatterned Charge Heterogeneities via Vapor Deposition of Aminosilanes. *Langmuir*, 10725-10733.

Coluccio, L. M. (1984). Phalloidin enhances actin assmebly by preventing monomer dissociation. *Journal of Cell Biology*, 529-535.

Cooper, G. (2000). *The Cell: a molecular approcah.*

D Tranchida, S. P. (2006). Some experimental issues of AFM tip blind estimation: the effect of noise and resolution. *Measurement Science and Technology*.

Dinara Sabola, S. T. (2017). Influence of scanning rate on quality of AFM image: Study of surface statistical metrics. *Microscopy Research and Technique*, 1328-1336.

Enrica Caló, V. V. (2014). Biomedical applications of hydrogels: A review of patents and commecial products. *European Polymer Journal*, 252-267.

F. Atamny, A. (1995). Direct imaging of the tip shape by AFM. *Surface Science*, L314-L318.

F. L. Leite, L. H. (2007). The Atomic Force Spectroscopy as a Tool to Investigate Surface. *Modern Research and Educational Topics in Microscopy*, 747-757.

Hansma, D. R. (1990). Atomic Force Microscopy. *Physics Today*, 23-30.

Hongda Wang, R. B. (2002). Glutaraldehyde modified mica: a new surface for atomic force microscopy of chromatin. *Biophysical Journal*, 3619-3625.

Hooke, R. (1678). *Lectures de Potentia Restitutiva, Or of Spring Explaining the Power of Springing Bodies.* London: The Royal Society.

I.E.Dzyaloshinskii, E. L. (1992). The general theory of van der Waals forces. *Perspectives in Theoretical Physics*, 443-492.

Isegrády, B. L. (2004). The effect of phalloidin and jasplakinolide on the flexibility and thermal stability of actin filaments. *FEBS Letters*, 163-166.

JKwiatkowski, D. (1999). Functions of gelsolin: motility, signaling, apoptosis, cancer. *Current Opinion in Cell Biology*, 103-108.

Kawamura, Y. O. (2016). *Hydrogels of Cytoskeletal Proteins: Preparation, Structure and Emergent Function.* Cham, Heidelberg, New York, Dordrecht, London: Spinger International Publishing.

Kopecek, J. (2009). Hydrogels From Soft Contact Lenses and Implants To Self-Assembled Nanomaterials. *Journal of Polymer Science A: polymer Chemistry*, 5929-5946.

L. Zitzler, S. H. (2002). Capillary forces in tapping mode atomic force microscopy. *Pysical Review B*.

Langer, N. P. (2006). Hydrogels in Biology and Medicine: From Molecular Principles to Bionanotechnology. *Advanced Materials*, 1345-1360.

Li, H.-Q. (1997, April 24). *The Common AFM Modes*. Retrieved from University of Guelph: http://www.chembio.uoguelph.ca/educmat/chm729/afm/details.htm

Liu, Y. X. (2010). Self-Assembled DNA Hydrogels with Designable Thermal and Enzymatic Responsiveness. *Advanced Materials*, 1117-1121.

M Kopycinska-Müller, R. G. (2006). Contact mechanics and tip shape in AFM-based nanomechanical measurements. *Ultramicroscopy*, 466-474.

Marina Naldi, E. V. (2009). Self-assembly of biomolecules: AFM study of F-actin on unstructured and nanostrucutred surfaces. *Nanoscale Imaging, Sensing, and Actuation for Biomedical Applications VI.* SPIE.

Michael Melak, M. P. (2017). Actin visualization at a glance. *Journal of Cell Science*, 525-530.

Monika Fritz, M. R. (1995). Imaging Globular and Filamentous Proteins in Physiological Buffer Solutions with Tapping Mode Atomic Force Microscopy. *Langmuir*, 3529-3535.

Oliver Lieleg, K. R. (2011). Biological Hydrogels as Selective Diffusion Barriers. *Trends in Cellular Biology*, 543-551.

Paulo, R. G. (1999). Attractive and repulsive tip-sample interaction regimes in tapping-mode atomic force microscopy. *Physical Review B*, 4961.

Shivani Sharma, H. Z. (2013). Correlative nanoscale imaging of actin filaments and their complexes. *Nanoscalce*, 5692-5702.

Soong Ho Um, J. B. (2006). Enzyme-catalysed assembly of DNA hydrogel. *Nature Materials*, 797-801.

Stephen P. Jackson, J. B. (2009). The DNA-damage response in human biology and disease. *Nature*, 1071-1078.

Taiji Ikawa, F. H. (2007). Molecular Scale Imaging of F-Actin Assemblies Immobilized on a Photopolymer Surface. *Physical Review Letters*.

Wiesendanger, R. (1994). *Scanning Probe Microscopy and Spectroscopy: Methods and Applications.* Cambridge: Cambridge Unversity Press.

Y. Martin, C. C. (1987). Atomic force microscope–force mapping and profiling on a sub 100-Å scale. *Journal of Applied Physics*, 4723.

APPENDIX: OPERATIONAL PROCEDURE FOR AFM EXPERIMENTS

The atomic force microscope system used for these experiments is the Veeco Dimension 3100 SPM System with NanoScope IV Controller (shown in figure 12). The software used with the system is the Nanoscope SPM version 5.31 software package that was bundled with the device by Veeco. The following is the step by step procedure for the operation of the Dimension 3100 SPM System with NanoScope IV Controller that was used in the imaging experiments described in this paper.

1. Open the Nanoscope SPM 5.31 software package from the desktop.

2. Click the Real Time Icon ⬚ to start the microscope. After initialization the controller will be online with a red LED illuminated on the front face. There will be two main windows displayed on the screens: On the left side is the Nanoscope Control window with all control settings, and on the right side the Nanoscope Image window with all of the image and signal displays.

3. Check Microscope Mode in the Other Controls panel. This is where the mode of operation is selected. To change to tapping mode, click Microscope Mode and hold, choose tapping mode from the list.
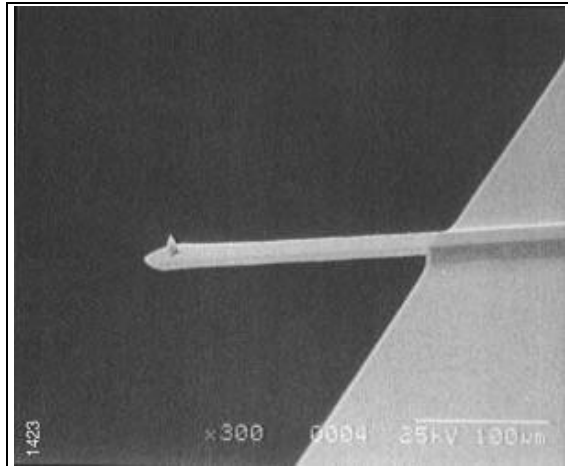

Figure 31: The etched single crystal silicon probe (TESP) that was used in the imaging experiments described in this work.

4. Check that the right probe is loaded for the AFM tapping mode. Tapping mode uses an etched single crystal silicon probe (TESP), as seen in figure 31.

5. Check the photodiode signals in the Nanoscope Image window on the right screen. For tapping mode the sum should be set at ~2 volts, the vertical deflection signal should be zero, and the red laser dot should be centered on the photodetector. The two knobs located to the left of the controller are used to adjust the signals. Make sure the controller is locked with the screw on the right side loosened.

6. Now the system is ready for the sample to be loaded. Before loading, it must be ensured that there is enough spacing between the sample holder surface and the AFM probe to fit the sample. It is advised to allow at least a spacing of 2-3 mm between your sample surface and the AFM probe when loading.

7. To raise the probe, click Focus Surface icon and then a Focus Surface window will pop up. Rolling the trackball up while pressing the Focus button will increase the height of the scanner with the probe. The sample may now be loaded and the vacuum toggle switched on to hold the sample in place during movement and imaging. The trackball is now used to move the piezo stage with the mounted sample underneath the AFM probe tip. Now exit the focus surface window by clicking ok.

8. Now the tip can be located and adjusted in the software. Click on the locate tip icon to open the locate tip window. The tip can then be centered on the cantilever under the cross hairs using the two knobs at the left of the optical objective of the microscope. Focus on the tip end of the cantilever using the trackball while pressing

the focus button. Adjust under zoom out first, then under zoom in, and adjust the illumination setting using left/right arrow keys to get a clear view of the tip.

9. Now we need lower the scanner close to the sample surface to get a good focus on it. Click on the focus surface ▣ icon. In the focus surface window choose zoom out and focus on surface. Find the fuzzy image of the cantilever on the right screen and adjust illumination to get a good view. Roll the trackball downward while pressing the focus button to lower the scanner with the probe. When the probe is getting close to the sample surface, two red spots of laser reflection will be visible on either side of the cantilever, both moving toward the cantilever as it is lowered. When the two spots approach to the edges of the cantilever, the probe is very close to the surface and you should be able to observe surface features and debris. By marking the surface of the substrate where the sample is deposited with a fine red marker, it is easy to locate at this distance my manipulating the trackball until the red spot becomes viewable in the focus surface window. Once the red spot is located adjust the height of the probe using the trackball focus button until the features of the spot are in focus. The zoom in setting can be used for fine focusing. The desired image site is ready to be moved under the crosshairs using the trackball. Lowering the scanner must be performed carefully as it is possible to lower the probe into the sample surface, thus damaging the tip and requiring replacement of the equipment. If the sum signal begins falling, then the probe is too close to the surface and the scanner should be raised.

10. The plastic hood can now be closed in order to reduce acoustic noise before imaging.

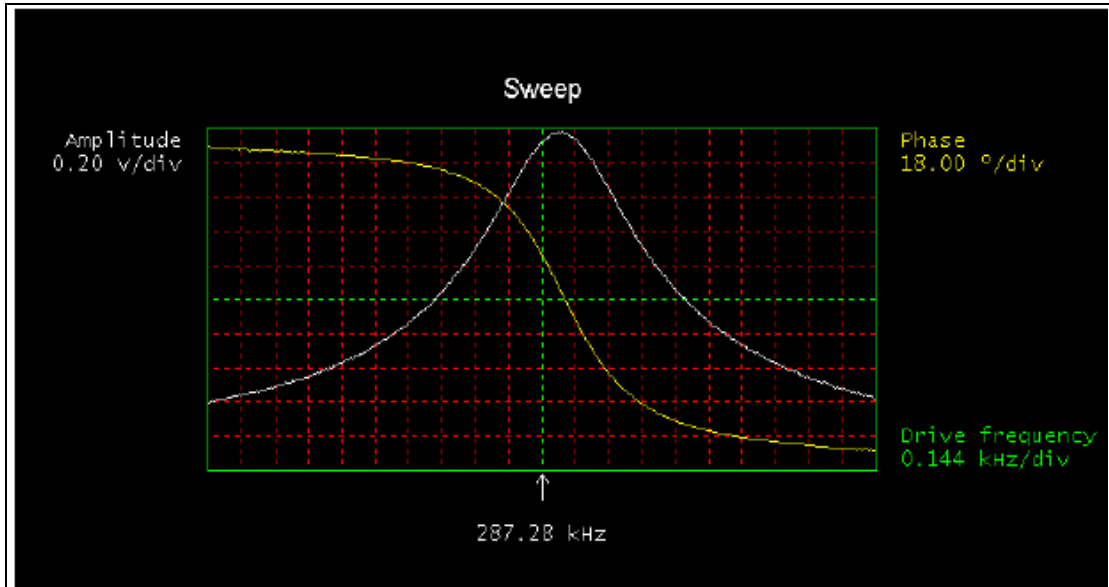11. Now it is time to tune the cantilever to the proper resonant frequency. Clicking on

Figure 32: The amplitude and phase curves that should be displayed after tuning the cantilever to its resonance frequency. The amplitude should be a smooth Gaussian curve and the phase should be smooth and sigmoidal.

the cantilever tune icon ⎍ opens the tuning window. Clicking on the auto tune button will prompt a display that the cantilever is tuning, and the display will disappear once the auto tune is done. Amplitude and phase curves will appear on the right monitor with the proper resonance frequency as shown in figure 32. The amplitude should be represented by a smooth and symmetrical Gaussian curve and the phase should be observed as a smooth sigmoidal (s-shaped) curve. If the curves are very uneven or the amplitude curve has more than one peak, then the cantilever may be damaged, dirty, or misaligned and the probe needs to be realigned or

replaced. When tuning is complete the image mode button may be clicked to quit the cantilever tune menu.

12. The Nanoscope control menu (imaged in figure 33) allows the user to set AFM scanning conditions. The initial scanning parameters must first be set in the scan controls panel. Set the initial scan size to 1 μm, x and y offsets to zero, and the scan
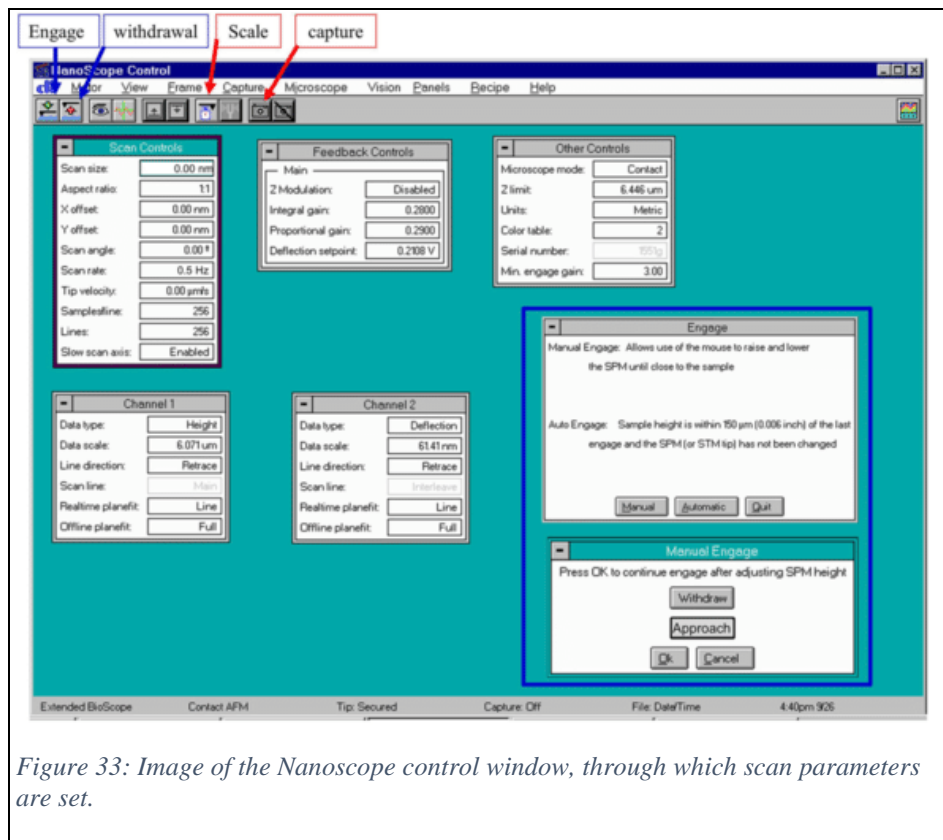

Figure 33: Image of the Nanoscope control window, through which scan parameters are set.

angle to zero. The slow scan axis should be enabled to restrict scanning to desired area. In the channel one panel, the data type should be set to height, line direction set to trace, real time plane fit to line, offline plane fit to full, and the high pass filter and low pass filter should both be set to off. In the feedback controls panel, the integral grain should be set to 0.4, the proportion grain to 0.6, and the scan rate to

1 Hz. Though the default scan rate is 2 Hz, the slower rate allows for a better signal to noise ratio and a higher quality image (Dinara Sabola, 2017).

13. At this stage the probe is ready to be brought into contact with the sample surface. Make sure the hood is closed to reduce acoustic noise. The engage icon ![engage icon] may now be clicked to begin stepping the probe tip down onto the surface. At the bottom of the NanoScope control window, a status bar will show the motors driving distance. The distance will slowly adjust until it reaches about 90 μm. If this value is much higher than 100 μm, then the tip will fail to engage due to the large tip to surface distance .If this occurs then the engage command should be ended by clicking the abort button on the engage window. The previous steps will then have to be repeated.

14. Scanning parameters need to be optimized at this juncture. Using the scope ![scope icon] mode by clicking the scope ![scope mode icon] mode icon to analyze the height and amplitude (labelled trace and retrace), one can make sure that the two values are tracking each other. The trace and retrace lines should be very similar since they are the same value, only in opposite directions. If the lines are not similar, amplitude set point, scan rate, and gain must be adjusted. The amplitude set point and the scan rate should be decreased until the lines look similar. Gain controls can be increased to make the trace and retrace more similar but after a certain amount of increase noise will begin to interfere with the measurement. Clicking the image mode icon takes the user back to the image window after making sure that the trace and retrace lines are reliably tracking.

15. Now the scan size is set to 3 μm and the aspect ratio set to 1:1, since these are reasonable dimensions for the visualization of single actin filaments. The zoom in and zoom out functions may be used to select the desired scanning area. Due to the stress experienced by the piezo crystals, the scan area position will not be exactly accurate.

16. After the desired scan area is chosen it is time to capture an image of the sample. The capture tab should be selected and the capture filename option selected. The desired filename should be entered and the next scan begins it will have the chosen filename. Clicking the capture icon will begin the image scan. The frame up icon or the frame down icon can be selected to begin the image capture at the bottom or top of the scan window respectively. The file extension is in a three digit format (e.g. .001) and each time an image is captured the software will increase the extension by 1 (.001 goes to .002, etc.). The status bar at the bottom of the window should now read *capture on* and when the scan is complete it will read *capture done*. The scan can be ended at any time by clicking the capture abort icon and the image capture will be cancelled. If the scanning parameters are changed during a scan, the software will wait to capture until the scan line reaches the top or bottom of the window (depending on if frame up or frame down is chosen) and starts with the next complete image. The status bar at the bottom will read *capture next* while waiting to begin the next image capture. The captured image is recorded in the local capture directory for offline operations/analysis.

17. After images have been collected, the scanner probe can raised for easy sample removal. Clicking the withdraw icon will raise the scanner away from the sample surface. It is recommended to click withdraw at least four times to avoid touching the probe during sample removal. The vacuum toggle should be switched off before removing the sample.

18. Clicking the image icon in the upper left corner of the Nanoscope control window will open the image window, where images can be investigated with various functions allowing for height/distance measurements, topological analysis, and artifact correction. By selecting the export function the image may be converted and exported as a TIFF image, JPEG, or ASCII file.

19. When imaging is complete, the acoustic hood should be closed and the Nanoscope software shut down by selecting file and exit. The red LED on the front face of the scanner should now be off, and the system is ready to be shut down.